



UNIVERSITY OF THESSALY
SCHOOL OF ENGINEERING
DEPARTMENT OF MECHANICAL ENGINEERING

Diploma Thesis

**Simulation of Additive Manufacturing
(3-D Printing)**

by

SYMEON KOIMTZIDIS

SUBMITTED IN PARTIAL FULFILMENT OF THE
REQUIREMENTS FOR DIPLOMA IN MECHANICAL ENGINEERING
2022

© 2022 Symeon Koimtzidis

The approval of the Diploma Thesis by the Department of Mechanical Engineering, School of Engineering, University of Thessaly does not imply acceptance of the author's views (N. 5343/32 αρ. 202 παρ. 2).

Approved by the Three Members of the Advisory Committee:

First Member (Supervisor)

Professor Nikolaos Aravas
Department of Mechanical Engineering, University of Thessaly

Second Member

Dr. Ioanna Papadioti
Department of Mechanical Engineering, University of Thessaly

Third Member

Professor Gregory Haidemenopoulos
Department of Mechanical Engineering, University of Thessaly

Abstract

Simulation of additive manufacturing

Symeon Koimtzidis

Supervisor: Professor N. Aravas

Additive manufacturing is a manufacturing process, where material is fused together layer by layer until the final geometry is formed. This is achieved by heating a thin layer of powdered metal with a laser beam until it melts and fuses with the base material or the previous layer. The molten material subsequently solidifies and a fully dense layer is formed. Such a process requires the development of high temperatures and the constant and rapid addition of layers leads to a process of thermal cycling. This thermal process inevitably leads to the development of residual stresses in the printed part and also influences the phases of the metal which may develop. This work is concerned with the simulation of the temperature field that develops during the AM process. The relevant analysis was performed with the use of the Abaqus/ Explicit solver and the UMATHT subroutine.

Keywords: Additive Manufacturing; Finite Element Method;

Acknowledgements

First and foremost, I would like to express my sincere gratitude towards Professor Nikolaos Aravas, the supervisor of my thesis, who offered me the opportunity to work on this intriguing topic.

I would also like to express my deepest appreciation to Dr. Ioanna Papadioti for providing the basis of the finite element model, as well as her continuous guidance and involvement with this thesis.

Moreover, I wish to thank Dr. John Aristeidakis and Marios Sotiriou for their invaluable assistance regarding the metallurgical aspects of additive manufacturing.

Lastly, I want to thank my whole family for their moral and material support throughout my years in the University of Thessaly.

Contents

| | |
|---|-----------|
| Abstract | vi |
| Acknowledgements | viii |
| List of Figures | x |
| List of Tables | xii |
| Introduction | 1 |
| 1 Heat Transfer Theory | 5 |
| 1.1 Heat transfer | 5 |
| 1.2 Heat Conduction | 6 |
| 1.3 Thermal Conductivity, Diffusivity and Specific Heat | 7 |
| 1.4 Heat Generation | 8 |
| 1.5 General Heat Conduction Equation | 9 |
| 1.6 Heat Convection | 11 |
| 1.7 Thermal Radiation | 11 |
| 1.8 Boundary and Initial conditions | 13 |
| 2 Methodology of the Finite Element Model | 15 |
| 2.1 Overview | 15 |
| 2.2 Mesh Description | 16 |
| 2.2.1 The Quiet Element Method | 16 |
| 2.2.2 Element Activation Process | 16 |
| 2.3 Thermal Problem | 18 |
| 2.3.1 Energy Balance in an Element | 18 |
| 2.3.2 Heat Generation with regard to Latent Heat | 18 |
| 2.3.3 Heat Generation from the Laser Heat Source | 19 |
| 2.3.4 Boundary Conditions / Heat losses | 20 |
| 2.3.5 Modelling Metal Powder | 23 |

| | |
|---|-----------|
| 3 Heat Transfer Model Application: a case study in 316L austenitic stainless steel | 27 |
| 3.1 Description of the Analysis | 27 |
| 3.2 Parameters of the Analysis and Material Properties | 28 |
| 3.3 Fine Mesh: Model-1 | 30 |
| 3.3.1 Overview | 30 |
| 3.3.2 Results | 31 |
| 3.4 Coarse Mesh: Model-2 | 32 |
| 3.4.1 Overview | 32 |
| 3.4.2 Results from Model-2 | 34 |
| 3.5 Complete 2-D Wall: Model-3 | 36 |
| 3.5.1 Overview | 36 |
| 3.5.2 Results from Model-3 | 38 |
| 3.6 Simulating the Effect of Metal Powder: Model-4 | 40 |
| 3.6.1 Overview | 40 |
| 3.6.2 Results from Model-4 | 41 |
| Discussion and Conclusions | 45 |
| Bibliography | 47 |

List of Figures

| | | |
|------|--|----|
| 1.1 | Three-dimensional medium. From [1] | 7 |
| 1.2 | Differential control volume in Cartesian coordinates. From [1] | 9 |
| 1.3 | Heat exchange, a) at a surface, b) between a surface and larger surrounding. From [2] | 13 |
| 2.1 | Elements in blue are active, while the white ones are inactive. | 17 |
| 2.2 | Representation of a double ellipsoidal source. For the simple ellipsoidal, $a_2 = a_1$. | 19 |
| 2.3 | Example of element activation. Convection and radiation B.C. are applied to the faces with green. Active elements are in blue while inactive ones have dashed borders. | 22 |
| 2.4 | Conduction in semi infinite medium with known temperature at the boundary. | 25 |
| 2.5 | Element activation adjustment for powder layer and powder B.C. | 25 |
| 3.1 | Material Properties based on temperature | 29 |
| 3.2 | Model-1, Fine mesh. | 30 |
| 3.3 | Model-1, zoom in at node locations | 31 |
| 3.4 | Model-1, Temperature history of certain nodes. The sixth image is a closer look at the single heating phase of Node 101046. | 32 |
| 3.5 | Geometry of Model-2 | 33 |
| 3.6 | Model-2 Node locations | 33 |
| 3.7 | Temperature history at certain nodes of Model-2. | 34 |
| 3.8 | Activation Times for two elements. The value 1 stands for element activation, while 0 means than an element is inactive. | 35 |
| 3.9 | Left: Element activation status, where red means active and blue inactive. Right: temperature contours at the same time as the images on the left. | 36 |
| 3.10 | Model-3 Geometry | 37 |
| 3.11 | Model 3 Node locations | 38 |
| 3.12 | Temperature history from model-3 at two nodes of its substrate. | 38 |

| | | |
|------|--|----|
| 3.13 | Temperature histories at three nodes of the wall section from model-3. The right bottom image is a zoom-in for the first heating phase of node 11742. . . | 39 |
| 3.14 | Temperature contour plots from Model-3 at different times during the same idle phase. | 39 |
| 3.15 | 13 Model-4 geometry and node locations | 41 |
| 3.16 | Model-4 at time = 10.0022 seconds. Top: temperature contours. Bottom left: elements with red are active with solid properties. Right: elements with red are active with powder properties. | 42 |
| 3.17 | Time graphs showing the state of two elements, element 26 at the top and element 476 at the bottom. On the left is their status as active elements with powder properties, while on the right is their status as active elements with proper metal properties. | 42 |
| 3.18 | Contour Plots of model-4 at different times | 43 |
| 3.19 | Temperature history of nodes 26 and 77. | 44 |
| 3.20 | Temperature history of nodes 485 and 994. | 44 |
| 3.21 | First heating at the node 485. | 44 |

List of Tables

2.1 Parameters used for the calculation of k_{eff} 24

3.1 Basic Parameters of the analysis 28

Introduction

Parts with increasingly complex geometries and high dimensional precision are becoming ever more crucial in several fields, ranging from the aerospace and automotive industry, to the medical and energy sectors. At the same time, it is also essential that these parts have high performance and can function at a plethora of harsh environments, from high altitudes to the inside of a blood vessel. More traditional manufacturing processes are challenged by this and may even sometime fall short of producing answers for the above demands. Nevertheless, these requirements may be fulfilled by a relatively newer production method, additive manufacturing (AM). The most prominent capability of AM is in its capacity to produce parts of significant complexity when compared to moulding or machining and this is due to the nature of its process.

At its core AM is a fairly straightforward process and shares some of its basic principles with welding. Initially, a thin layer of fine metal powder is laid on top of a base and subsequently a focused laser beam, selectively hits the powder and melts it in order to fuse it with the base material. This powder layer and base are referred to as the powder bed which is in an enclosed space, surrounded by inert gas (usually argon) in order to prevent the molten metal from oxidizing. Once, the laser has scanned all the required spots the construction of the first layer is considered complete. Then this process begins cycle and a miniscule layer at a time the whole part is constructed. Thanks to this layered method of construction AM can tackle the creation of surfaces with complex curves and angles, while also making no distinction between the inside and outside surface of the processed part. For example, titanium alloys are preferred due to their high mechanical properties, yet these very properties make them challenging and time consuming to machine, not to mention expensive. So, such parts may be more efficiently constructed through AM. Nonetheless, AM has its share of challenges.

Before, analyzing these challenges it is important to note the process parameters that are of immediate significance to AM. These are the travel velocity, intensity and hatch spacing of the laser beam as well as the thickness of each layer. These particular parameters are often expressed through the term of energy density. The laser spot diameter, the thermophysical properties of the printed metal and the scan strategy are also important factors. Their immediate effects are seen on the melt pool, where a bad set up may lead to insufficient melting of the powder or conversely evaporation. This is why a lot of research is conducted in order to determine favourable combinations of the above parameters for each metal alloy.

Another challenge arrives as a consequence of the rapid thermal cycling and significant temperatures that occur during AM. These lead initially to thermal stresses, which complicate the first stages of the construction process, during which the part may be fairly feeble due to its incomplete geometry. A common countermeasure for this, is the construction of temporary supports, which are built alongside the printed part. More troubling however, are the residual stresses which often develop and can significantly weaken a part's mechanical properties. They can also lead to part distortion, which for parts of high dimensional precision is a catastrophic defect.

With the above in mind, it becomes apparent that the monitoring of the transient thermal field that develops during the AM process, is of great interest. With this information the stresses, deformations, as well as the phases of the printed metal which may develop, can be predicted. In order to determine this thermal field, a simulation of the AM process is presented. It is based on the Selective Laser Melting (SLM) process specifically.

This analysis employs a two-dimensional finite element technique developed on the Abaqus software [3], in order to predict the thermal field that develops due to the moving heat source. The chosen metal for this model was an AISI 316L austenitic stainless steel. There was also an effort to simulate as many layers as possible in order to fit this model's parameters to those of physical experiments, such as [8] and those mentioned in [11]. Such an analysis can quickly become very demanding based on how many layers are constructed and how large the printed surface's overall geometry is. To account for these rising demands, a modified version of the quiet element method was used as will be discussed in Chapter 2. This required an accurate prediction of the melt pool's length, so based to the research of [12], a simple ellipsoidal heat source was employed, which is also how the effects of the laser are introduced to the analysis. The model of the heat source was according to [5].

The process of AM combines a plethora of physical phenomena, which occur simultaneously and in order to produce a comprehensive model at this stage assumptions had to be made. Two notable simplifications were, the steady density of the steel despite temperature and phase changes as well as the two-dimensional model itself. Nonetheless, great emphasis was put on the modelling of the boundary conditions, in the form combined convection and radiation. More specifically convection was modelled in order to account for the phenomena of forced convection which can occur above a significantly heated surface, like the one above the melt pool created by the laser. This was done in accordance with the research of [ref Gouge]. Radiation was also considered, regardless of the computational demand of its highly non-linear nature. This is because of the important heat losses it introduces to the system at high temperatures, further accelerating the already high cooling rates that occur once the laser departs from a region. Lastly, another version of the model was produced, this time taking into account the effects of the metal dust, while also calculating its thermal properties which differ from those of proper metal. This powder proved to noticeably influence the

temperatures that the model predicts for the melt pool. In addition, a conduction boundary condition was developed around it, accounting for the fact that such models are submerged inside the powder bed, with only their top surface being exposed.

In the context of this thesis, the fundamentals of heat transfer theory briefly described during Chapter 1. In Chapter 2 the method according to which the finite element model was employed, is discussed. This includes, the modification of the quiet element method, the expression of the boundary conditions and the heat source as well as the necessary calculations in order to calculate the properties of powdered metal.

Chapter 1

Heat Transfer Theory

In this chapter a brief overview of the heat transfer theory is presented. Its focus is around the major mechanisms of heat transfer that are relevant to this analysis, mainly conduction, convection and radiation. Conduction influences the way the temperature field will evolve inside the model, while the other two influence how the heated system dissipates that heat to its environment. Most of what is written is based on the books of [1] and [2].

1.1 Heat transfer

Heat is the form of energy which is transferred from one system to another, that is at a lower temperature. This process continues until temperature equilibrium is reached and the amount of energy transferred, as well as the rate at which this was achieved are important in this field of study. This process is in accordance with the laws of thermodynamics:

1. *First law*: The rate at which a system's energy changes must be equal to the rate at which energy is transferred to and from the system.

$$\left(\begin{array}{c} \textit{Total energy} \\ \textit{entering the} \\ \textit{system} \end{array} \right) - \left(\begin{array}{c} \textit{Total energy} \\ \textit{departing from} \\ \textit{the system} \end{array} \right) = \left(\begin{array}{c} \textit{Change in the} \\ \textit{total energy of} \\ \textit{the system} \end{array} \right) \quad (1.1)$$

2. *Second law*: Heat is always transferred from a system of high temperature to another with lower temperature.

The above-mentioned equation (1.1) can be more specifically expressed for the purposes of heat transfer as follows:

$$\underbrace{Q_{in} - Q_{out}}_{\text{Net heat transfer}} + \underbrace{\Delta E_{generated}}_{\text{Heat generation}} = \underbrace{\Delta E_{thermal,system}}_{\text{Change in the system's thermal energy}} \quad [J] \quad (1.2)$$

Heat transfer can occur through three main mechanisms conduction, convection and radiation. In addition, heat may be released or absorbed as the result of a process occurring in the system, like a phase change. All these methods respect the previously mentioned laws of thermodynamics.

1.2 Heat Conduction

The process of *conduction* occurs in solids, liquids and gases and is based on how energy is exchanged among the molecules of a substance. It is influenced by the temperature difference between the points it occurs and the greater this difference is, the faster the rate of heat conduction. In contrast, this rate of heat transfer decreases as the distance Δx , between the points on which it is measured, increases. Moreover, when two surfaces that have a temperature imbalance come into contact, they come to an equilibrium quicker when their contact area A , is greater. Lastly, conduction is influenced by the physical properties of the material through which it occurs and this is expressed by the materials *thermal conductivity* k , measured in $[\frac{W}{mK}]$.

Heat conduction is expressed as a formula through *Fourier's law*:

$$\dot{Q}_{conduction} = -kA \frac{dT}{dx} \quad (1.3)$$

Where, $\dot{Q}_{conduction}$ is the rate of heat transfer in [W] and $\frac{dT}{dx}$ is the temperature gradient with regard to the x-axis.

It is a common convention for $\dot{Q}_{conduction}$ to be positive when it is transferred along the positive direction of the axis. So, the negative sign is there to ensure this convention, while at the same time heat is transferred from a place of high to one of low temperature.

At this point it should be noted that heat transfer is a vector quantity. This means that in order to adequately describe it, one needs to define its magnitude and direction. This in turn leads to a temperature field that can vary in space and time, meaning that temperature now has four variables, $T=T(x,y,z,t)$. Where x,y and z are coordinates based on an orthonormal coordinate system and t is the time variable.

The previously mentioned time dependency creates two ways of characterization for heat transfer based on the change of temperature through time, or the lack thereof. A heat transfer problem that remains unchanged as time passes is classified as a *steady state* problem. When the temperature field displays time dependency, then such a problem is referred to as *transient state* problem.

In order to express Fourier's law as a general relation of heat conduction, a three-dimensional

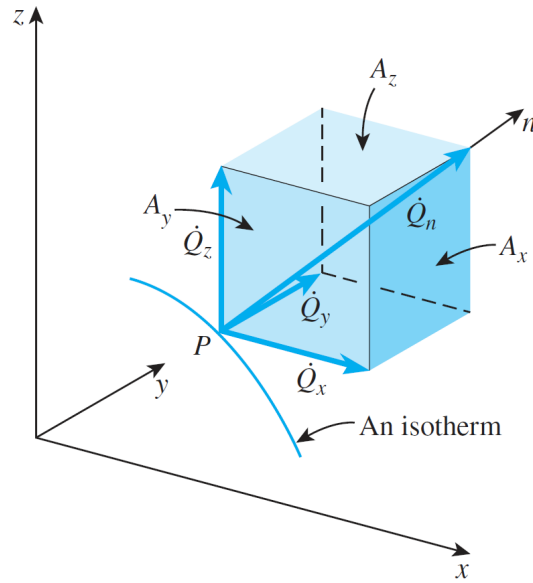


Figure 1.1: Three-dimensional medium. From [1]

medium should be considered, as displayed in Figure 1.1. Each one of its surfaces is considered an *isothermal surface*, meaning that there is no temperature change on it. The heat transfer vector at a given point P on such a surface must be perpendicular to the surface and point towards the direction of decreasing temperature. If \mathbf{n} is the normal of the isothermal surface at point P, then the rate of heat conduction at that point in accordance with Fourier's law is:

$$\dot{Q}_n = -kA \frac{dT}{dn} [W] \quad (1.4)$$

The heat conduction vector may be analyzed in terms of its components in rectangular coordinates as:

$$\dot{\mathbf{Q}}_n = \dot{Q}_x \mathbf{i} + \dot{Q}_y \mathbf{j} + \dot{Q}_z \mathbf{k} \quad (1.5)$$

Where, \mathbf{i} , \mathbf{j} and \mathbf{k} are the unit vectors and \dot{Q}_x , \dot{Q}_y and \dot{Q}_z are the magnitudes of heat transfer rates in the directions of the x,y and z axis respectively. Fourier's law may be applied to each according to equation 1.4, where \mathbf{n} may be substituted with x,y or z.

$$\dot{Q}_x = -kA_x \frac{dT}{dx} \quad , \quad \dot{Q}_y = -kA_y \frac{dT}{dy} \quad , \quad \dot{Q}_z = -kA_z \frac{dT}{dz} \quad (1.6)$$

Here A_x , A_y and A_z are the heat conduction areas normal to each axis as shown in Figure 1.1.

1.3 Thermal Conductivity, Diffusivity and Specific Heat

Since thermal conductivity has just been used in the previous equations, here would be a fitting place to present some of a material's properties, which influence the way it conducts heat.

- *Specific Heat* c_p , in $[\frac{kJ}{kgK}]$: or more accurately specific heat capacity under constant pressure, expresses a materials capacity to store thermal energy per unit mass at a certain temperature.
- *Thermal Conductivity* k , in $[\frac{W}{mK}]$: is used to measure the rate at which thermal energy is transferred per unit thickness of the mean of conduction, per unit area and per unit of temperature. It is a property that helps distinguish a good conductor from and insulator of heat.

For metal alloys, thermal conductivity is sensitive to the composition of the alloy and usually the thermal conductivity is lower than that of any of the pure metals that constitute it.

- *Thermal diffusivity* a , in $[\frac{m^2}{s}]$: Initially it should be noted that the product of density and specific heat, ρc_p , in $[\frac{J}{m^3K}]$, defines the amount of heat stored per unit volume at a certain temperature. Then the ratio of conductivity k to ρc_p is defined as thermal diffusivity a :

$$a = \frac{\text{Heat conduction}}{\text{Heat storage}} = \frac{k}{\rho c_p} \quad (1.7)$$

This property describes how rapidly heat can diffuse through a given material. So, the greater thermal diffusivity is, the faster heat can propagate through a material.

All the above properties can vary based on temperature and also for different phases of the same material. This was also taken into consideration in this analysis, as will be described in Chapter 3.

1.4 Heat Generation

All forms of energy processes have heat as at the very least a by-product. This means that it is possible that mechanical, electrical, nuclear or chemical energy may be converted into heat inside the volume of a medium, through which heat can be conducted. Such a phenomenon is taken into account through the heat generation term of a system.

The above is not limited to the production of heat, but also the absorption of it as well. An example for each case would be an exothermic and an endothermic reaction respectively. More relevant to this analysis is the release or absorption of heat that occurs during the phase change of a medium, which is referred to as *latent energy* (or more commonly latent heat).

As can be omitted from all the above, heat generation is a *volumetric phenomenon*. It occurs throughout the whole volume of the relevant medium. Therefore, the rate of

heat generation is measured per unit volume and expressed by the term \dot{e}_{gen} , in $[\frac{W}{m^3}]$. When the variation of heat generation with respect to its position is known, then the total rate of heat generation in a medium of volume V is:

$$\dot{E}_{gen} = \int_V \dot{e}_{gen} dV \quad (1.8)$$

1.5 General Heat Conduction Equation

To develop such an equation, first a rectangular element of infinitesimal dimensions Δx , Δy and Δz is considered as a *control volume*, as shown in Figure 1.2. The density of the material inside it is ρ and its specific heat is c . The energy balance in this element during a small, time interval Δt is expressed as:

$$\left(\begin{array}{c} \text{Rate of heat} \\ \text{conduction at} \\ x, y \text{ and } z \end{array} \right) - \left(\begin{array}{c} \text{Rate of heat} \\ \text{conduction at} \\ x + \Delta x, y + \Delta y \\ \text{and } z + \Delta z \end{array} \right) + \left(\begin{array}{c} \text{Rate of heat} \\ \text{generation inside} \\ \text{the element} \end{array} \right) = \left(\begin{array}{c} \text{Rate of change in} \\ \text{the energy content} \\ \text{inside the element} \end{array} \right)$$

Or

$$\dot{Q}_x + \dot{Q}_y + \dot{Q}_z - (\dot{Q}_{x+\Delta x} + \dot{Q}_{y+\Delta y} + \dot{Q}_{z+\Delta z}) + \dot{E}_{gen,el} = \frac{\Delta E_{el}}{\Delta t} \quad (1.9)$$

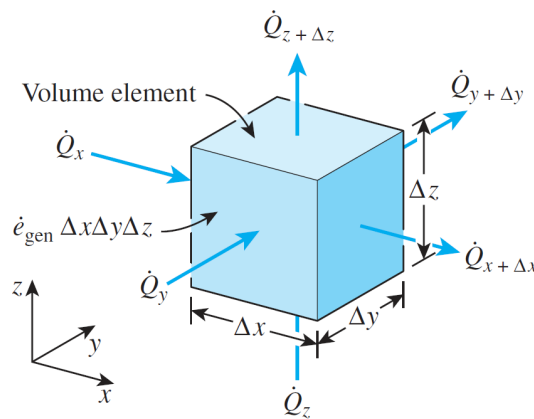


Figure 1.2: Differential control volume in Cartesian coordinates. From [1]

The volume of the element is $V_{el} = \Delta x \Delta y \Delta z$. The change of the energy and the rate of heat generated inside the element can be expressed as:

$$\Delta E_{el} = E_{t+\Delta t} - E_t = mc(T_{t+\Delta t} - T_t) = \rho c \Delta x \Delta y \Delta z (T_{t+\Delta t} - T_t) \quad (1.10)$$

$$\dot{E}_{gen,el} = \dot{e}_{gen} \Delta x \Delta y \Delta z \quad (1.11)$$

By substituting (1.10) and (1.11) into (1.9) and subsequently dividing by $\Delta x \Delta y \Delta z$:

$$\begin{aligned} & - \frac{1}{\Delta y \Delta z} \frac{\dot{Q}_{x+\Delta x} - \dot{Q}_x}{\Delta x} - \frac{1}{\Delta x \Delta z} \frac{\dot{Q}_{y+\Delta y} - \dot{Q}_y}{\Delta y} - \frac{1}{\Delta y \Delta x} \frac{\dot{Q}_{z+\Delta z} - \dot{Q}_z}{\Delta z} + \\ & + \dot{e}_{gen} = \rho c \frac{T_{t+\Delta t} - T_t}{\Delta t} \end{aligned} \quad (1.12)$$

It should be noted that the element exchanges heat with its environment through the faces A_x, A_y and A_z in the directions of x,y and z respectively. From the elements geometry it can be derived that $A_x = \Delta y \Delta z$, $A_y = \Delta x \Delta z$ and $A_z = \Delta y \Delta x$ and by taking the limit of $\Delta x, \Delta y, \Delta z$ and Δt towards 0, the definition of the derivative and Fourier's law:

$$\lim_{\Delta x \rightarrow 0} \frac{1}{\Delta y \Delta z} \frac{\dot{Q}_{x+\Delta x} - \dot{Q}_x}{\Delta x} = \frac{1}{\Delta y \Delta z} \frac{\partial \dot{Q}_x}{\partial x} = \frac{1}{\Delta y \Delta z} \frac{\partial}{\partial x} \left(-k \Delta y \Delta z \frac{\partial T}{\partial x} \right) = -\frac{\partial}{\partial x} \left(k \frac{\partial T}{\partial x} \right)$$

$$\lim_{\Delta y \rightarrow 0} \frac{1}{\Delta x \Delta z} \frac{\dot{Q}_{y+\Delta y} - \dot{Q}_y}{\Delta y} = \frac{1}{\Delta x \Delta z} \frac{\partial \dot{Q}_y}{\partial y} = \frac{1}{\Delta x \Delta z} \frac{\partial}{\partial y} \left(-k \Delta x \Delta z \frac{\partial T}{\partial y} \right) = -\frac{\partial}{\partial y} \left(k \frac{\partial T}{\partial y} \right)$$

$$\lim_{\Delta z \rightarrow 0} \frac{1}{\Delta x \Delta y} \frac{\dot{Q}_{z+\Delta z} - \dot{Q}_z}{\Delta z} = \frac{1}{\Delta x \Delta y} \frac{\partial \dot{Q}_z}{\partial z} = \frac{1}{\Delta x \Delta y} \frac{\partial}{\partial z} \left(-k \Delta x \Delta y \frac{\partial T}{\partial z} \right) = -\frac{\partial}{\partial z} \left(k \frac{\partial T}{\partial z} \right)$$

Thus, equation (1.12) becomes:

$$\frac{\partial}{\partial x} \left(k \frac{\partial T}{\partial x} \right) + \frac{\partial}{\partial y} \left(k \frac{\partial T}{\partial y} \right) + \frac{\partial}{\partial z} \left(k \frac{\partial T}{\partial z} \right) + \dot{e}_{gen} = \rho c \frac{\partial T}{\partial t} \quad (1.13)$$

This is the general heat conduction equation expressed in rectangular coordinates. For a *homogeneous* and *isotropic* material k does not change with regard to location so:

$$\boxed{\frac{\partial^2 T}{\partial^2 x} + \frac{\partial^2 T}{\partial^2 y} + \frac{\partial^2 T}{\partial^2 z} + \frac{\dot{e}_{gen}}{k} = \frac{1}{a} \frac{\partial T}{\partial t}} \quad (1.14)$$

Where, $a = \frac{k}{\rho c}$ is the material's thermal diffusivity. This equation is also known as the *Fourier-Biot* equation.

1.6 Heat Convection

Convection is the form of heat transfer which occurs between a solid and the adjacent fluid (gas or liquid), which may be in motion. It is also the dominant heat transfer mechanism in fluids. If the fluid is in motion, then heat transfer through convection is increased proportionally with its velocity. In case the fluid is stationary the heat convection accounts mainly for the heat conduction between the fluids molecules. These two cases lead to two types of convection:

1. *Forced Convection*: when the fluid is forced to flow over the solid's surface, thus moving constantly and with significant velocity.
2. *Natural convection*: the only fluid motion is due to the buoyancy forces. These occur as the fluid directly adjacent to the solid's surface temperature exchanges heat through conduction with the solid. This leads to temperature variation, which causes density differences and subsequently buoyancy forces.

The rate of heat transferred via convection was measured to be proportional to the temperature difference between the surface of the solid and the mean temperature in the bulk of the fluid, as well as the area of the surface itself. Convection is expressed by *Newton's law of cooling*:

$$\dot{Q}_{conv} = hA_s(T_s - T_\infty) \quad (1.15)$$

The convection heat transfer coefficient h in $[\frac{W}{m^2K}]$: is an experimentally determined parameter and is not a property of the fluid. Its value depends on the surface geometry, properties of the fluid, nature of the fluid's motion and the bulk fluid's velocity.

A_s in $[m^2]$ is the area through which convective heat transfer occurs.

T_s is the temperature on that surface.

T_∞ is the temperature of the fluid away from the area of heat exchange, which is typically unaffected.

1.7 Thermal Radiation

In contrast to conduction and convection, heat transfer by radiation does not require an intervening medium. Radiation is a form of energy emitted by all matter and takes the form of electromagnetic waves (photons). It is the result of the change in the configuration of electrons of the atoms or molecules of a material.

Radiation is a volumetric phenomenon and all solids, liquids and gases emit, absorb or transmit it. However, for solids it is typically considered a surface phenomenon,

as most solids are typically regarded as opaque to thermal radiation. This is done because the radiation emitted by the regions in their interior never reaches the surface and the radiation incident on such bodies seldomly penetrates further than the surface.

Based on the *Stefan-Boltzmann law*, the rate at which a surface at temperature T_s , in [K], can emit thermal radiation, is described by:

$$\dot{Q}_{emit} = \epsilon \sigma A_s T_s^4 \quad (1.16)$$

Emissivity ϵ : is a property that describes how efficiently a surface can emit thermal radiation, so it has values ranging from $0 \leq \epsilon \leq 1$. A surface with $\epsilon = 1$ is considered a *black-body* and is the idealized emitter whose thermal radiation is called black-body radiation. This value depends on the quality of that surface and may also be effected by the temperature of it.

Similar to emissivity, *absorptivity* α is another property that influences thermal radiation. It describes the ratio of radiation energy that a surface can absorb, so it too ranges from $\alpha = 0$ to $\alpha = 1$. A black-body is a perfect absorber as well ($\alpha = 1$). In addition, *Kirchhoff's law of radiation* states that the emissivity and absorptivity of a surface at a given temperature and wavelength are equal.

The rate at which a surface absorbs radiations is determined from:

$$\dot{Q}_{abs} = \alpha \dot{Q}_{incident} \quad (1.17)$$

The difference between the rate of radiation emitted and absorbed by the surface, is the net heat exchanged via thermal radiation. The formula for calculating the net rate of radiation heat transferred between a surface of thermodynamic temperature T_s and a surrounding far larger surface at temperature T_{surr} is:

$$\dot{Q}_{rad} = \epsilon \sigma A_s (T_s^4 - T_{surr}^4) \quad (1.18)$$

Where, ϵ is the emissivity of the smaller surface and A_s its area. This equation is unaffected if a gas (like air) is in-between those two surfaces.

Radiation heat transfer can occur alongside convection as well as conduction, as it is displayed in Figure (1.3). It is common that a solid's free surface exchanges heat with convection and radiation at the same time, so the net rate of heat exchange is their sum:

$$h_{combined} = h_{conv} + h_{rad} = h_{conv} + \epsilon \sigma (T_s + T_{surr})(T_s^2 + T_{surr}^2) \quad (1.19)$$

So that:

$$\dot{Q}_{total} = h_{combined} A_s (T_s - T_{surr}) \quad (1.20)$$

Radiation tends to become the dominant form of heat transfer at high temperature, while at lower ones it is convection who is the main contributor.

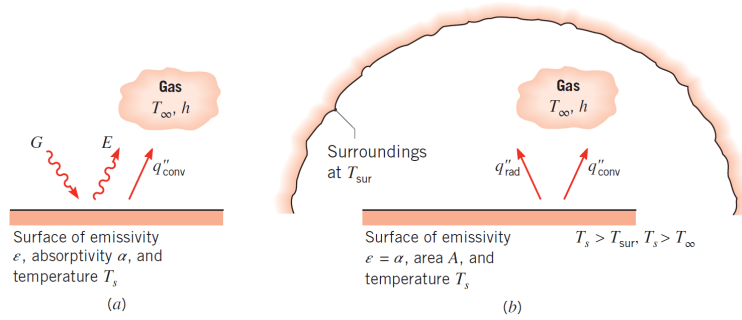


Figure 1.3: Heat exchange, a) at a surface, b) between a surface and larger surrounding. From [2]

1.8 Boundary and Initial conditions

The differential equation (1.18) satisfies the energy balance inside a differential element which is inside a medium of heat transfer. To further this description, it is appropriate to assign boundary and initial conditions to this problem.

An initial condition may be the temperature field of that medium at $t=0$:

$$T(x, y, z, t = 0) = f(x, y, z)$$

As for the boundary conditions, in order to adequately describe a problem, two need to be provided for every direction of the coordinate system that heat transfer can occur. Therefore, two boundary conditions need to be specified for a one-dimensional problem, four for a two-dimensional one and six for a three-dimensional problem. Some examples are provided below, yet boundary conditions are not limited to these ones:

- Specified temperature at a boundary: $T(x_1, y, z) = T_1$
- Specified heat flux $\dot{q} = -k \frac{\partial T}{\partial x} \Big|_{x=x_1}$

The last boundary condition can specifically be in the form of:

- Insulated boundary: $\frac{\partial T}{\partial x}\Big|_{x=x_1} = 0$
- Convection Boundary condition: $\dot{q} = -k \frac{\partial T}{\partial x}\Big|_{x=x_1} = h(T_\infty - T|_{x=x_1})$
- Radiation Boundary condition: $\dot{q} = -k \frac{\partial T}{\partial x}\Big|_{x=x_1} = \epsilon\sigma(T_{surr}^4 - T^4|_{x=x_1})$
- A combination of convection and radiation.

The convection and radiation boundary conditions are written as if the surface at x_1 is facing the origin of the x-axis. For the boundary facing the opposite direction, in order to maintain the convention around the positive direction of \dot{Q} , the boundary conditions need to change sign.

Chapter 2

Methodology of the Finite Element Model

2.1 Overview

For the purposes of this analysis a two-dimensional finite element model was created, using the Abaqus software. This software allows for, the modelling of the analysis, the solution of the problem as well as the visualization of its results. Abaqus Explicit was specifically employed in this instance as this model requires the simulation of transient loads, such as the moving heat source of the laser.

The first step for a finite element analysis is the creation of a suitable mesh. As the name additive manufacturing implies, more material is progressively deposited onto the already existing one, so this would call for dynamic meshing (a mesh that is evolving). However, this was avoided with the implementation of the quiet element method, which allows a certain dynamic behaviour to the mesh. According to this method, the whole mesh is generated from the start and material properties as well as boundary conditions are applied to each element progressively and accordingly. This property assignment is referred to as the activation of an element and it was based on the relative location of the element's integration points with regard to the moving laser (heat source). Moreover, the effects of metal powder were taken into consideration, both as an intermediate state of an element and as a boundary condition.

In order to achieve this, several subroutines of the Abaqus software were used as well as some complimentary user subroutines. They were namely UMATHT, DFLUX, MPC and they were supplemented by subroutines that accounted for the laser's location, its active or inactive state, the value of latent heat and the temperature dependent values of the metal's and powder's thermal conductivity and specific heat.

2.2 Mesh Description

2.2.1 The Quiet Element Method

According to the *quiet element method*, initially the whole mesh is generated and all elements are considered inactive and shall be progressively activated. The properties of an inactive element are assigned very small values, in order to limit its influence during the current increment of the analysis. This method allows for mesh generation to be a standard procedure, in contrast to dynamic mesh generation, thus simplifying the analysis. However, inactive elements are still part of the analysis and may have unintended effects as well as, extend the computation time.

In order to prevent this risk, further simplify the analysis and save time, a modified version of this method is employed. The properties of inactive elements are assigned zero values, such elements do not influence the current increment of the analysis. Moreover, the temperature at nodes that are not part of active elements remains constant and equal to the initial one. When a node is shared between an active and an inactive element, the temperature there may change according to what the simulation dictates and is no longer fixed. This is achieved through the use of the MPC subroutine in conjunction with other user subroutines, which will be described in the following paragraphs.

As the heat source moves and material is added, the elements considered part of the deposited material are activated. That is when the appropriate properties are assigned to them. As this is a thermal analysis these properties are thermal conductivity (k) and specific heat capacity (c_p). Also, once an element has been activated, it cannot return back to an inactive state.

This modification is reasonable as elements that are inactive are essentially consisted of the air surrounding the metal, upon which a new layer of material is being deposited. As will be described later, the effects of said air will be accounted for through the convection boundary condition and thus the temperature field of it does not further influence that of the printed part.

2.2.2 Element Activation Process

An element is being activated based on the relative location of its integration points, to the heat source or more specifically the laser spot. The scanning strategy of the laser is to begin melting metal powder from the bottom left corner and move towards the right one. Then it pauses for a few seconds, this is referred to as idle time and

during this time in SLM printing the next layer of powder is placed. After this time the laser is returned to its initial position and repeats the same process for the above layer.

Initially, the location of the laser is defined through the user defined subroutine KLASER. This subroutine has two parts, during its first part it calculates the (x_{laser}, y_{laser}) coordinates of the laser spot during the scanning phase, taking its travel speed into consideration. During the second part it simply fixes the laser at a given spot for the duration of the idle time.

Now the relative coordinates (ξ, η) of an integration point relative to the laser are calculated:

$$\begin{aligned}\xi &= x_{laser} - x_{int\ pt} \\ \eta &= y_{laser} - y_{int\ pt}\end{aligned}\tag{2.1}$$

If $\eta > tol \times dy$ and $|\xi| \leq a$ then the element to which this integration points belong to, is activated.

Where:

- tol is an arbitrary tolerance, set at 10^{-4}
- dy is the dimension of an element in the y-direction
- a is the radius of the laser spot

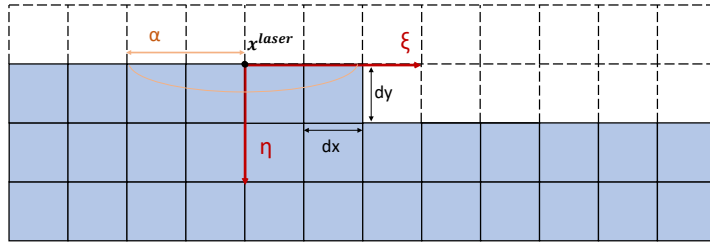


Figure 2.1: Elements in blue are active, while the white ones are inactive.

Through this algorithm, all the inactive elements at a given increment of the analysis are found and through the subroutine MPC their temperature is fixed at the initial temperature. Also, their thermal conductivity k_{quiet} and specific heat capacity $c_{p_{quiet}}$ are given by the equations:

$$\begin{aligned}k_{quiet} &= s_k k, \text{ with } s_k = 0 \\ c_{p_{quiet}} &= s_k c_p, \text{ with } s_{c_p} = 0\end{aligned}\tag{2.2}$$

2.3 Thermal Problem

2.3.1 Energy Balance in an Element

When there is a temperature imbalance between elements, heat will flow in the appropriate direction and when these elements are representing parts of a solid, this will be achieved through conduction. As mentioned in Chapter 1 this will be done in accordance with equation (1.13):

$$\nabla \cdot (\mathbf{k} \cdot \nabla(T)) + \dot{e}_{gen} = \rho c_p \frac{\partial T}{\partial t} \quad (2.3)$$

In this analysis all materials shall be considered as homogeneous and isotropic so $\mathbf{k} = k\delta$ (with δ being the second order unit tensor) so equation (2.3) becomes the Fourier-Biot equation:

$$k \nabla^2(T) + \dot{e}_{gen} = \rho c_p \frac{\partial T}{\partial t} \quad (2.4)$$

With:

- k , being thermal conductivity in $\frac{W}{m K}$
- \dot{e}_{gen} , the rate of heat generation per unit volume $\frac{W}{m^3}$
- ρ , density in $\frac{kg}{m^3}$
- c_p , specific heat in $\frac{J}{kg K}$

2.3.2 Heat Generation with regard to Latent Heat

The term \dot{e}_{gen} can consist of two parts, one is heat generated through the heat source and the other is heat absorbed or released through phase changes, in the form of latent heat.

Latent heat is considered as internal energy per unit mass U_l (T) and is assumed to vary smoothly from $U_l(T_{Solidus}) = 0$ to $U_l(T_{Liquidus}) = U_{latent}$ according to the following equation proposed by [4]:

$$U_l = U_{latent} \left[3 \left(\frac{T - T_S}{T_L - T_S} \right)^2 - 2 \left(\frac{T - T_L}{T_L - T_S} \right)^3 \right] \quad (2.5)$$

This equation also allows for the function's derivative to be zero at $T_{Solidus}$ and $T_{Liquidus}$:

$$\left. \frac{dU_l}{dT} \right|_{T=T_S} = \left. \frac{dU_l}{dT} \right|_{T=T_L} = 0 \quad (2.6)$$

Multiplying $U_l(T)$ with the density ρ and dividing by the increment time, it is converted into the rate of energy added per unit volume $[\frac{W}{m^3}]$:

$$\dot{e}_l = \rho \frac{\Delta U_l(T)}{\Delta t} \quad (2.7)$$

This may now be used as part of the \dot{e}_{gen} term at the appropriate temperature range of $(T_{Solidus}, T_{Liquidus})$.

2.3.3 Heat Generation from the Laser Heat Source

When the laser is active and traversing the printing area its energy input is modelled according to a *simple ellipsoid volumetric heat source*, as described in [5]:

$$\dot{e}_{laser} = \frac{6\sqrt{3}P}{abc\pi\sqrt{\pi}} e^{-3\left[\left(\frac{\xi}{a}\right)^2 + \left(\frac{\eta}{b}\right)^2 + \left(\frac{z}{c}\right)^2\right]} \quad (2.8)$$

Where (ξ, η, z) are the local coordinates of an integration point relative to the center of the ellipsoid and a, b and c are parameters of the ellipsoid as shown in Figure (2.2):

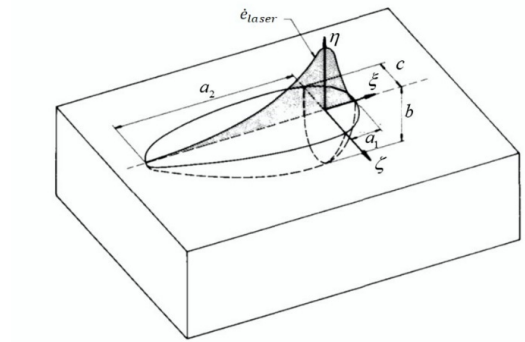


Figure 2.2: Representation of a double ellipsoidal source. For the simple ellipsoidal, $a_2 = a_1$.

The current model is two-dimensional, so the heat source is modified assuming that the mesh is a plane defined by the η and ξ axis and that all of the energy input in the plane defined by ζ and ξ is absorbed entirely.

$$\begin{aligned} \int_{-\infty}^{+\infty} \dot{e}_{laser} dz &= \frac{6\sqrt{3}P}{abc\pi\sqrt{\pi}} e^{-3\left[\left(\frac{\xi}{a}\right)^2 + \left(\frac{\eta}{b}\right)^2\right]} 2 \int_0^{+\infty} e^{-3\left(\frac{z}{c}\right)^2} dz = \\ &= \frac{6\sqrt{3}P}{abc\pi\sqrt{\pi}} e^{-3\left[\left(\frac{\xi}{a}\right)^2 + \left(\frac{\eta}{b}\right)^2\right]} 2 \frac{c\sqrt{\pi}}{2\sqrt{3}} \end{aligned} \quad (2.9)$$

Thus, the equation of heat the source for a two-dimensional mesh is:

$$\dot{e}_{laser} = \frac{6P}{ab\pi} e^{-3\left[\left(\frac{\xi}{a}\right)^2 + \left(\frac{\eta}{b}\right)^2\right]} \quad (2.10)$$

The parameters a and b were adjusted in order to describe the dimensions of the melt pool created by the laser. This energy input is introduced to the model via the DFLUX subroutine, which will be discussed later.

2.3.4 Boundary Conditions / Heat losses

For this model, boundary conditions are in the form of know heat flux at a given surface. This surface consists of the element faces that are on the outside of the model. In such areas heat is lost simultaneously due to convection and radiation. They are modelled as follows:

$$-\mathbf{q} \cdot \mathbf{n} = q_n = \text{know on } S \quad (2.11)$$

Where, q_n is the heat power flux at a point on the surface S and by convention is positive when heat enters the model. For convection:

$$q_c = -h(T - T_0) \quad (2.12)$$

Where:

- h is the convection coefficient (or film coefficient) of the surrounding gas.
- T_0 is the sink temperature ($27^\circ C$ in this case)
- T is the temperature on the surface at a given time (expressed in $^\circ C$).

The film coefficient was also modelled based on the research of [6] on hot-film *anemometry*. In essence, it was measured that h changes when directly above a surface that has substantially high temperatures, like those over the melt pool caused by the laser. This is due to high temperature differences in the fluid, which lead to high density differences and in turn substantial buoyancy forces and movement.

$$h(r) = h_{max}e^{Br} + h_0 \quad (2.13)$$

Where:

- r is the radial distance from the heat source
- h_{max} is the peak value of the film coefficient
- B is the exponential decay rate
- h_0 is the convective offset (base value of the film coefficient)

This calibration of the convection coefficient was performed in a circular area, whose radius was ten times the larger than the radius of the laser's spot. In addition, this area was centred at the location of the laser spot and moved along with it.

For radiation, the heat flux is:

$$q_r = -\sigma\epsilon [(T - T_z)^4 - (T_0 - T_z)^4] \quad (2.14)$$

Where:

- T_z is the absolute zero temperature (-273.15°C)
- ϵ is the emissivity of the material
- σ is the Stefan-Boltzmann constant $\sigma = 5.669 \times 10^{-8} \frac{W}{m^2(^{\circ}C)^4}$

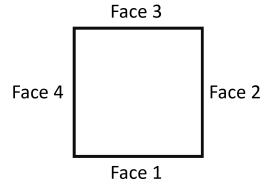
Now the sum of 2.14 and 2.12, is the total flux of the heat losses:

$$q_n = q_r + q_c \quad (2.15)$$

The open surfaces of the model that represent the material on top of which the rest will be deposited on, have this boundary condition imposed on them from the start. As material is added and the surface on the top evolves, the following algorithm is followed in order to appropriately apply the boundary conditions.

In Abaqus, each face of the square element is numbered as follows:

- Face 1: bottom surface
- Face 2: right surface
- Face 3: top surface
- Face 4: left surface



Initially a distinction is being made between active and inactive elements and the relative coordinates (ξ, η) of its integration points with regard to the laser spot are calculated. Where, x_0^{laser} is the starting x coordinate of the laser, x^{laser} is the present coordinate, dx and dy are the dimensions of an element and a is a parameter of the heat source (referencing the laser spot radius). Also, NW is the number of the first element to be activated, NOEL is the number of the elements this integration point belongs to and NUM is the total number of elements in each layer.

For an already active element

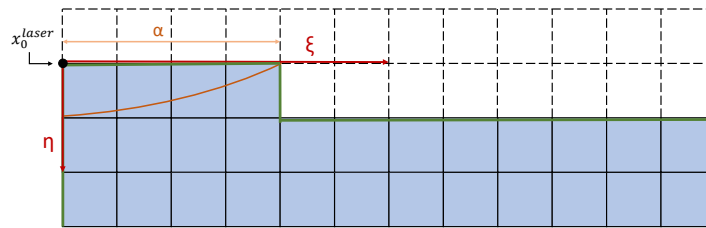
- If $|\eta| < dy$ and $x^{npt} < x^{laser} + a$, then the boundary conditions must be activated for face 3 of the elements this integration point belongs to.
- If $|\eta| < 2dy$ and $x^{npt} > x^{laser} + a$, then the boundary conditions are activated for face 3.

- If $\text{NOEL} > \text{NW}$ and $x^{npt} < x_0^{laser} + dx$, then the boundary conditions are activated for face 4.
- If $\text{NOEL} > \text{NW}$ and $x^{npt} > x_0^{laser} + (\text{NUM} - 1)dx$, then the boundary conditions are activated for face 2.

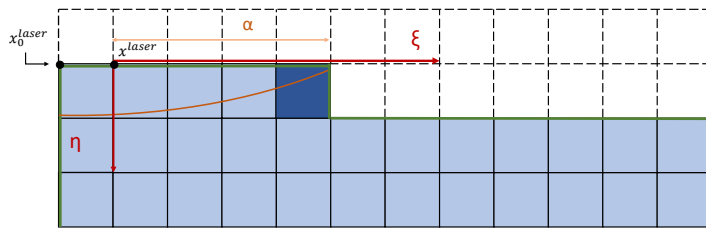
For an element which is set to activate during the current increment

- If $|\eta| < dy$, then the boundary conditions are activated for face 3.
- If $|\xi| + dx > a$, then the boundary conditions are activated for face 2.
- If $x^{npt} < x_0^{laser} + dx$, then the boundary conditions are activated for face 4.

An example of this is displayed in Figure (2.3). The element in dark blue is activated as the laser whose center is the intersection of the two red lines moves (x^{laser}). The green line represents the faces on which the convection and radiation boundary conditions are applied.



(a) Mesh at t_1



(b) Mesh at $t_2 > t_1$

Figure 2.3: Example of element activation. Convection and radiation B.C. are applied to the faces with green. Active elements are in blue while inactive ones have dashed borders.

The boundary conditions of the elements' faces, that are not impacted by the deposition of new material, are introduced via the RADIATE and FILM commands in the Abaqus main code and are considered separately. For the elements that are impacted, their boundary conditions are introduced through the DFLUX subroutine just like heat generation.

2.3.5 Modelling Metal Powder

The material which is deposited is initially in the form of fine powder, this powder is laid on top of the newly printed area during the idle time of the laser and then melted as it is hit by the laser. This powder also often surrounds the model and influences the boundary conditions. In order to measure its influence an altered version of the previous model was develop in order to account for the melting of powder as well as the powder boundary condition.

The powder was considered to be packed in an FCC formation with a packing coefficient of 0.7405, thus the density of it (ρ_{powder}) was considered to be 74.05% of the solid metal's density. The powder's specific heat ($c_{p_{powder}}$) was also considered as 74.05% of the solid metal's, as that of the air is insignificant in comparison to the metal. The *effective thermal conductivity of powder* k_{eff} was calculated according to the study of [7] and was obtained through the following calculations:

First it is required to calculate the effective powder emissivity ϵ_p :

$$\epsilon_H = \frac{\epsilon_s \left[2 + 3.082 \left(\frac{1-\phi}{\phi} \right)^2 \right]}{\epsilon_s \left[2 + 3.082 \left(\frac{1-\phi}{\phi} \right)^2 \right] - 1}, \quad A_H = \frac{0.908\phi^2}{1.908\phi^2 - 2\phi + 1},$$

$$\epsilon_p = A_H \epsilon_H + (1 - A_H) \epsilon_s \quad (2.16)$$

For FCC the porosity ϕ is 0.2595, ϵ_H is the solids emissivity, ϵ_H is the gap emissivity and A_H is the area fraction of the powder surface.

$$k_{eff} = k_g \left[J_1 + \sqrt{1 - \phi} \left(J_2 + \Lambda \frac{k_{contact}}{k_g} \right) \right]$$

$$J_1 = \left(1 - \sqrt{1 - \phi} \right) \left(1 + \frac{\phi k_R}{k_g} \right)$$

$$J_2 = (1 - \Lambda) \left(\frac{2}{1 - \frac{Bk_g}{k_s}} J_3 + \frac{k_R}{k_g} \right) \quad (2.17)$$

$$J_3 = \left[\frac{B}{\left(1 - \frac{Bk_g}{k_s} \right)^2} \left(1 - \frac{k_g}{k_s} \right) \ln \left(\frac{k_s}{Bk_g} \right) - \frac{B+1}{2} - \frac{B-1}{1 - \frac{Bk_g}{k_s}} \right]$$

Where:

$$B = 1.25 \left(\frac{1 - \phi}{\phi} \right)^{\frac{10}{9}}, \quad k_R = \frac{4\epsilon_p \sigma T^3 x_R}{1 - 0.132\epsilon_p} \text{ and} \quad (2.18)$$

$$k_{contact} = 18\Lambda k_s, \quad \text{for } \Lambda < 3 \cdot 10^{-4}$$

| Term | Description | Term | Description |
|---------------|--|-----------|--------------------------------------|
| $k_{contact}$ | Thermal conductivity between particles | Λ | Fractional contact area of particles |
| k_R | Thermal radiation | B | Deformation parameter |
| k_g | Thermal conductivity of the gas | σ | Stefan Boltzmann constant |
| k_s | Thermal conductivity of solid metal | x_R | Average powder diameter |

Table 2.1: Parameters used for the calculation of k_{eff}

For temperatures below $T_{Solidus}$, the powder's thermal conductivity was considered based on equation 2.17. For temperatures above that it smoothly transitions to the thermal conductivity of the liquid metal, using the phase fraction of the liquid as the weighting parameter. . Above $T_{Liquidus}$ both thermal conductivities were considered equal.

With the powder layer in mind, the first modification was in the top layer of elements. As shown in Figure 2.5 all the elements of the layer which is about to be hit by the laser are activated. This top layer is then divided into two types of element properties, those with the properties of the solid metal and those representing powder. As was mentioned there is no difference in their properties when either element type is above $T_{Liquidus}$, so the transition time between the two element types was chosen as the time when the laser spot has just past the element.

- If an element is inactive and $\eta > tol$, then an element is activated with the properties of powder.
- If $\eta > tol$ and $\xi > \alpha$, then that element's properties turn from those of powder to those of proper metal.

The boundary condition at the edge of the model, where heat is dissipated through conduction to the surrounding powder, was obtained from the analytical solution to the transient heat conduction through a semi infinite medium. with the properties of

metal powder, at a known surface temperature T_s . According to [1], the heat flux on the boundary can then be given analytically as:

$$q_s = \frac{k_{eff}}{\sqrt{\pi\alpha t}} (T_s - T_0) \tag{2.19}$$

Where T_s is the temperature on the interface of the built specimen with the surrounding powder and evolves according to the numerical solution of the heat equation in the modeled region as the process progresses. Also, $\alpha = \frac{k_{eff}}{\rho_{powder}c_{ppowder}}$ is the thermal diffusivity of the powder, ρ_{powder} is its density and $c_{ppowder}$ is its specific heat. T_s is the temperature in the surface between the powder and the element face and T_0 is the ambient temperature of the powder (considered 27°C). Lastly, t is the time duration for which heat has been dissipated through the semi-infinite medium, counting from the time that the element was initially activated. This boundary condition was applied to the sides and the bottom of the model and like the previous ones it was also introduced through the DFLUX subroutine.

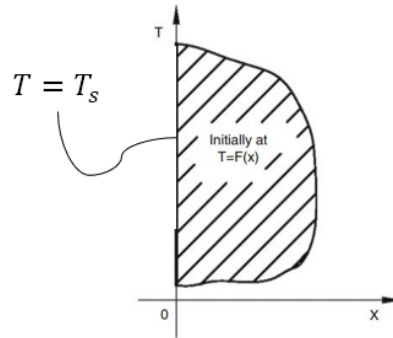


Figure 2.4: Conduction in semi infinite medium with known temperature at the boundary.

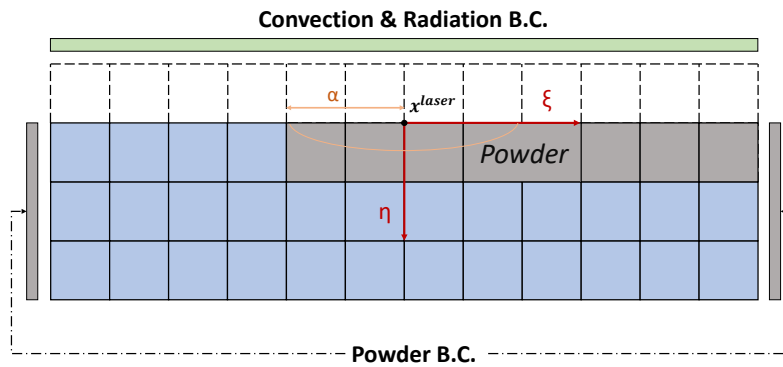


Figure 2.5: Element activation adjustment for powder layer and powder B.C.

Chapter 3

Heat Transfer Model Application: a case study in 316L austenitic stainless steel

3.1 Description of the Analysis

This analysis was performed in order to calibrate the model according to the experiments on SLM 3-D printing of [8]. There, a thin wall was constructed through the use of single layers on top of one another, this is in line with the two-dimensional nature of this model. The wall was 13mm wide and 13mm tall. It was printed at a speed of $v_s=675$ mm/s, with a layer thickness of $l=0.02$ mm and a laser power of $P=100$ W. In order to simulate this, a total of 650 layers would need to be deposited. This would require significant time as well as space in order to simulate. To avoid this, it was proposed to simulate the deposition of multiple layers at once, while maintaining the same energy density and having the same total energy input in the system. Energy density is calculated by the formula:

$$e_d = \frac{P}{v_s l h}, \text{ in } \left[\frac{J}{mm^3} \right] \quad (3.1)$$

Where:

- P is laser's power in [W].
- v_s is the laser's travel (or scanning) speed in [mm/s].
- l is the layer thickness, in [mm].
- h is the hatch spacing, in [mm]. Since it was built through single layers, h is assigned a unit value.

In a first stage, two models, Model-1 and Model -2 were created, they have the same overall geometry but have different element dimensions. This was done in order to check if the temperature field that would develop in each model would be similar and if so, then use the less dense mess to simulate the whole geometry of Bertsch's wall. For all models, the four-node linear elements DC2D4, for diffusive heat transfer were employed.

Regarding the *boundary conditions*:

- Models -1,-2 and -3 have the same boundary conditions applied to them. These are, a combined convection, radiation B.C. at the top, left and right surfaces of the model, while for the bottom surface only the convective heat losses where considered. Radiation heat losses were not considered for the bottom surface since the temperatures that develop there are fairly low and these loses may be ignored.
- For Model-4, the BC at the top surface was considered to be one of combined radiation and convection. The bottom, left and right surfaces were considered to be submerged inside the powder bed, so the powder BC was applied there, as described during subsection 2.3.5 .

3.2 Parameters of the Analysis and Material Properties

For every analyses these parameters remained consistent:

| Term | Value | Term | Value |
|--|--------------------------|-------------------------|-----------------------|
| Laser Power P | 100 W | $T_{Solidus}$ | 1379°C |
| Density ρ | 7.9 [$\frac{kg}{m^3}$] | $T_{Liquidus}$ | 1430°C |
| Convection coefficient h | 30 [$\frac{W}{m^2K}$] | Ambient temperature | 27°C |
| Convection coefficient above melt pool | 200 [$\frac{W}{m^2K}$] | Q_{latent} | 197.6 $\frac{kJ}{kg}$ |
| Emissivity ϵ | 0.4 | Emissivity of melt pool | 0.47 |

Table 3.1: Basic Parameters of the analysis

Emissivity typically changes based on temperature, yet for this analysis, two representative values where selected. The base value, 0.4, was chosen for the side surfaces that develop moderate temperatures, while the value 0.47 was assigned to the surfaces

at the top of the model where the metal reaches temperatures above $T_{Liquidus}$. This was performed in order to account for the changes of the emissivity's value once the material has been heated significantly.

The thermophysical properties of 316L austenitic stainless steel were calculated according to the work of [9]. A two-phase diffusion cell was considered as a representative structure, accounting for the austenitic and liquid phases. These calculations accounted for, the solidification process and the subsequent solid-state transformations, from 27°C to 2500°C . In this manner, $T_{Solidus}$, $T_{Liquidus}$, Q_{latent} , c_p and ρ were calculated. Thermal conductivity was based on the values from [10]. The properties of the powder were calculated based on what was described in Chapter 2, deriving from the same properties of solid steel. Also, this analysis accounted for the changes of k and c_p that occur along with changes in temperature.

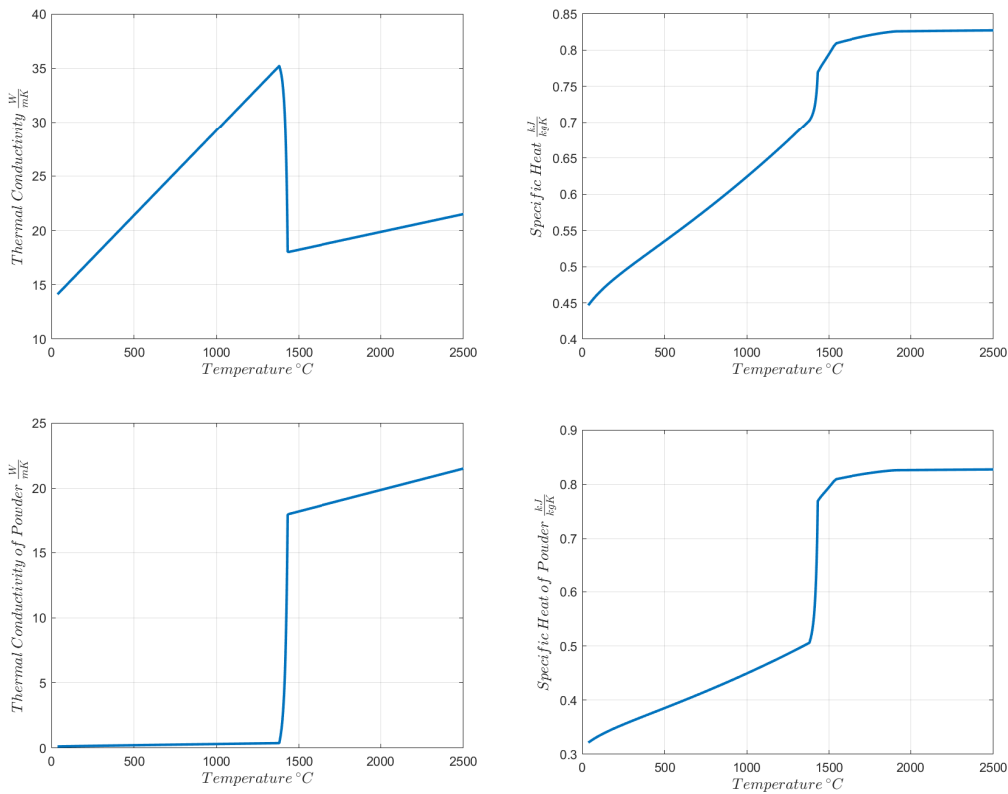


Figure 3.1: Material Properties based on temperature

3.3 Fine Mesh: Model-1

3.3.1 Overview

This model was designed in order to accurately simulate one layer of material per layer of wall elements. All the above parameters were employed, with the exception of metal powder, which was not considered during this analysis.

The geometry of model-1 is as shown in figure 4.2, with the dimensions of the substrate being 6mm in length and 10mm in height and the printed part, 3mm in length and 0.4mm in height. The nodes of the substrate had dimensions of $DX=0.06\text{mm}$ and $DY=0.1\text{mm}$, while those of the wall section had $DX=0.06$ $DY=0.02$. In total, the whole model consisted of 11,000 elements, 1,000 of which were assigned to the wall segment in order to simulate the printing of 20 layers, each 0.02mm thick. The laser's starting coordinates were $(x_0, y_0)=(1.5, 10)$ and it moved from left to right. The parameters of the volumetric heat source were $(a, b)=(0.04, 0.02)$, that was in order to align "a" with the spot radius and "b" with the layer thickness. The laser had a speed of $v_s=675$ mm/sec and its idle time was, $DTIDLE=10\text{sec}$ after every layer.

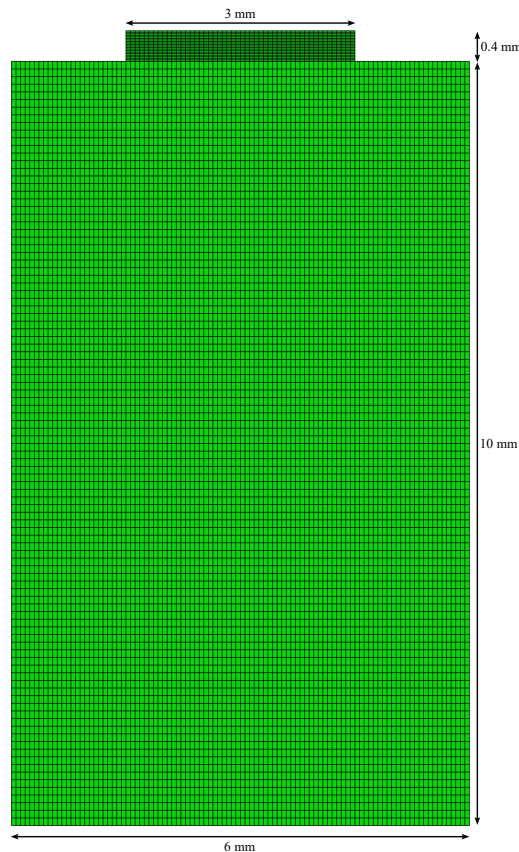


Figure 3.2: Model-1, Fine mesh.

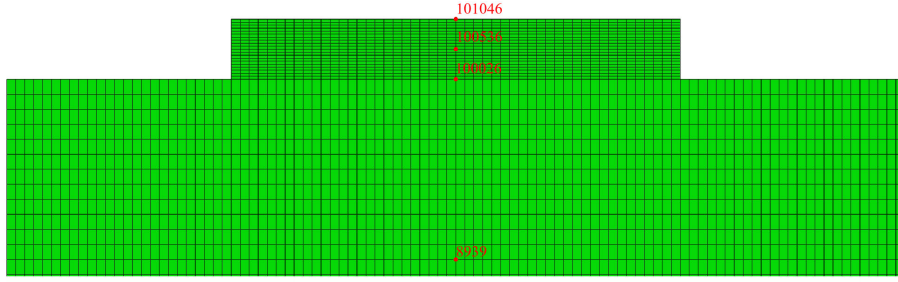


Figure 3.3: Model-1, zoom in at node locations

3.3.2 Results

Here the results of the aforementioned analysis are presented, displaying graphs that show the temperature history at certain nodes, whose location can be seen at Figure 3.3. Note that node number 51 is at the bottom of the substrate and that all nodes have the same x-coordinate, $x=3\text{mm}$.

From the temperature history of node 51 it can be confirmed that the temperatures at the bottom of the substrate remains low, so the radiation boundary condition has a negligible contribution to the heat flux. There, each laser scan can be seen as a small “slope” and the height of each slope is gradually decreasing. This shows a significant dissipation of the heat input from the boundaries of the substrate. Node 8939 is also in the substrate but closer to the heat source, at coordinates (3,8.8) and thus the influence of the energy input in the system is more pronounced. There, every scan can be clearly discerned and the high transient nature of the problem also becomes apparent. During every scan the temperature raises to a higher maximum and after every cooling phase it drops to its lowest temperature which is slightly elevated from the previous lowest temperature.

At the nodes of the wall 100536 and 101046, the significant gradient of the temperature field with regard to time can be observed. The lowest temperature is increasing slightly and the maximum one is decreasing the further from the heat source the node gets. In the sixth graph the rapid heating and cooling occurring during a single pass can be observed. The heating phase is almost linear, interrupted only during the phase change of the metal, where heat is absorbed in the form of latent energy. After the heating phase, cooling occurs immediately and at rapid pace due to the major diffusion of heat through conduction. However, once the temperature field has a more even spatial distribution, cooling slows down and is now based on the convection and radiation heat losses, which occur at slower rates.

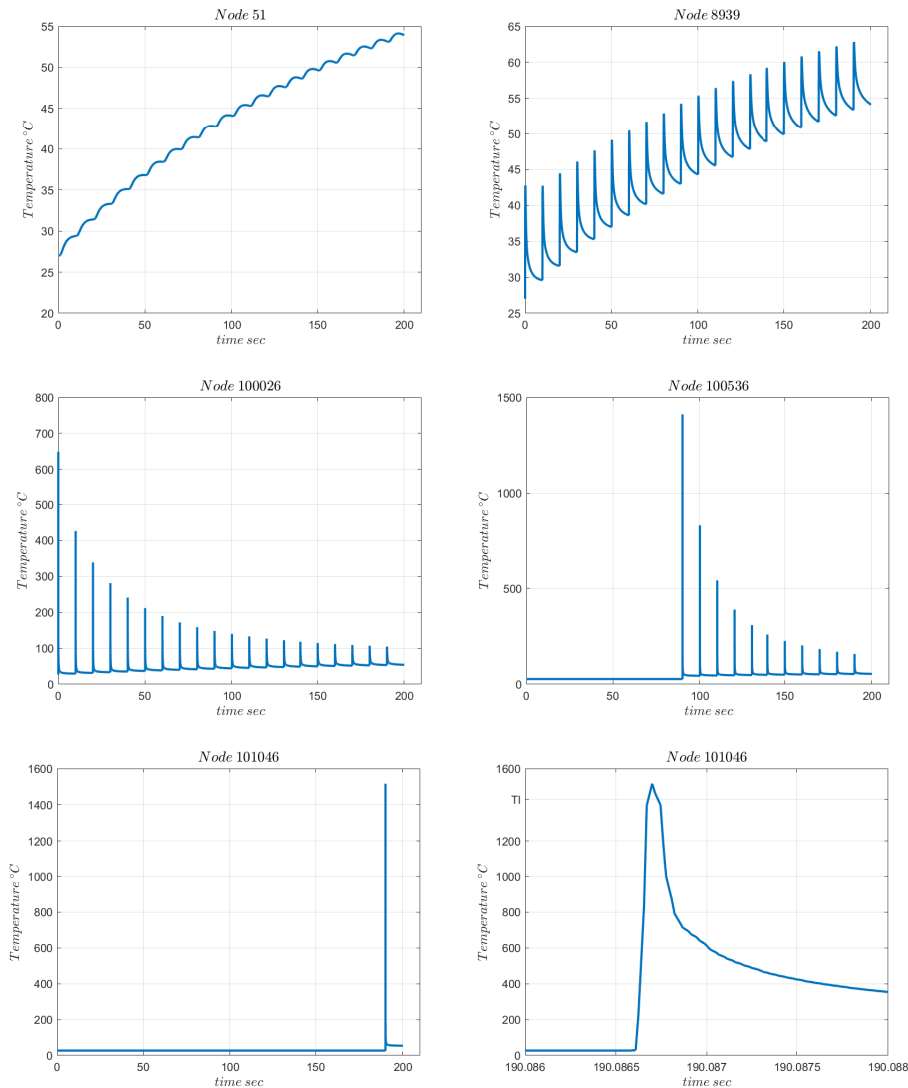


Figure 3.4: Model-1, Temperature history of certain nodes. The sixth image is a closer look at the single heating phase of Node 101046.

3.4 Coarse Mesh: Model-2

3.4.1 Overview

This model was created as an approximation of 10 layers being printed at once. It consisted of a total of 1,530 elements and 30 of them were assigned to the wall part. Its geometry can be seen in Figure (3.6). All the parameters mentioned at the start of the chapter, at table 3.1 were considered.

The following parameters were specific to this analysis:

- Laser speed: $v_s=67.5$ mm/sec

- Idle time of the laser: DTIDLE=100sec
- Laser starting location: $(x_0, y_0)=(1.5, 10)$
- Element dimensions: DX=0.2mm and DY=0.2mm

The parameters of the heat source were $a=0.4\text{mm}$ and $b=0.2\text{mm}$ while c was given a unit value.

The speed of the laser was assigned this value (67.5 mm/sec) in order to have equal energy density with model-1 and the idle time was 100 sec in order to ensure the same amount of energy is gained by the system in the same time as Model-1.

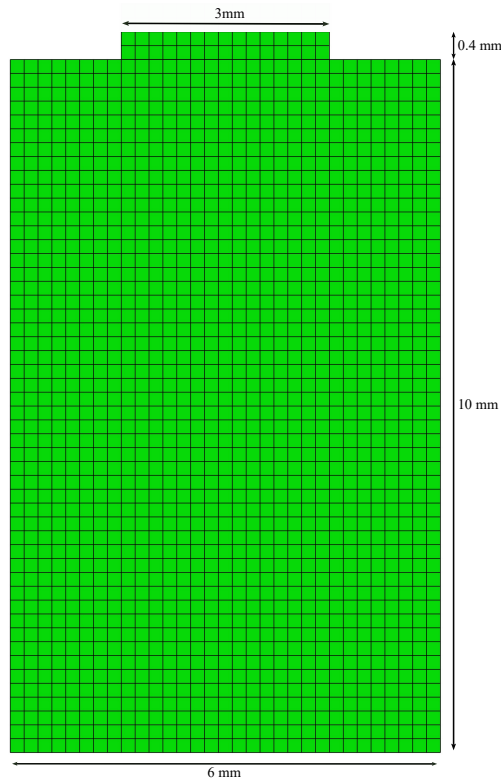


Figure 3.5: Geometry of Model-2

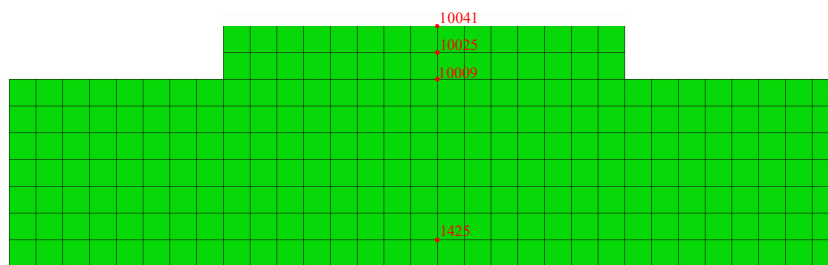


Figure 3.6: Model-2 Node locations

3.4.2 Results from Model-2

The following results were selected in the nodes whose location can be seen in Figure (3.6). They were also picked as closely as possible to the coordinates of the nodes shown for Model-1. In order to have a similar geometry with Model-1, only two layers were printed for a total of 0.4mm of added height. Here are also displayed graphs regarding the activation time of two elements which are at different layers.

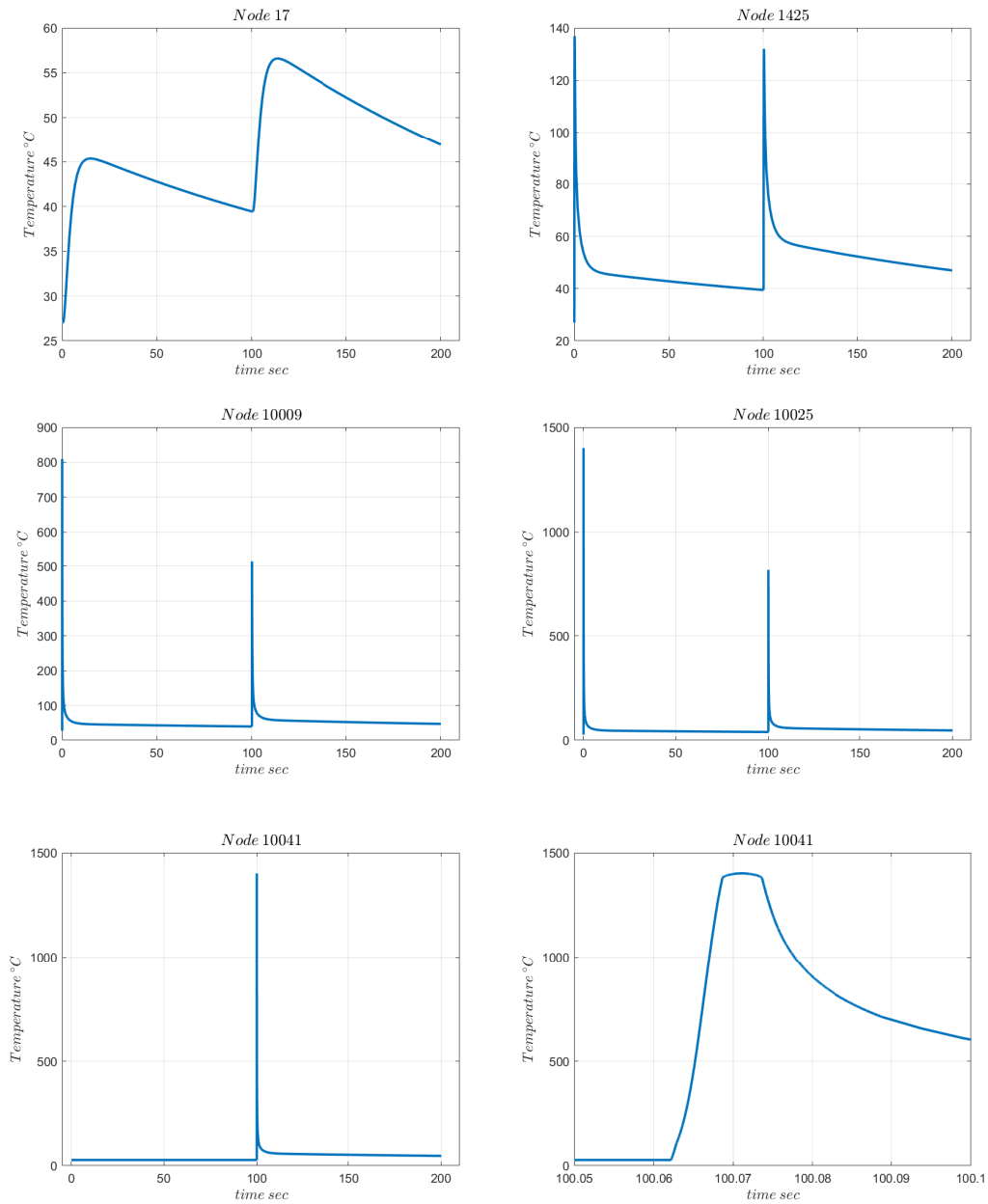


Figure 3.7: Temperature history at certain nodes of Model-2.

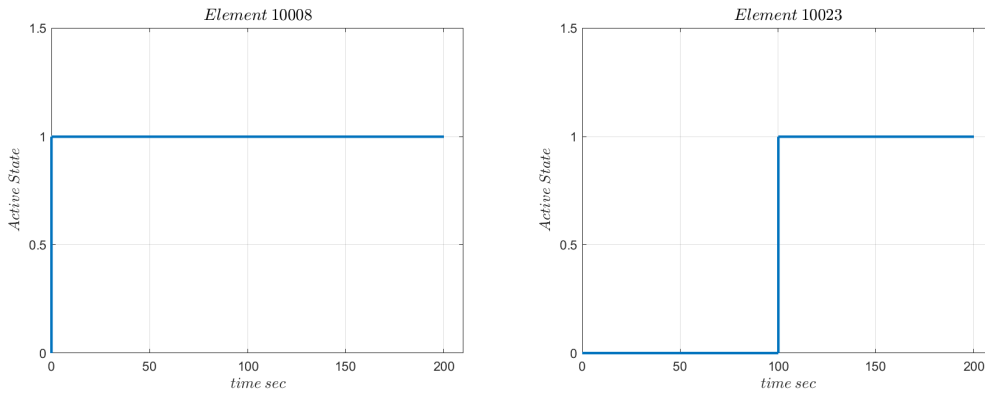


Figure 3.8: Activation Times for two elements. The value 1 stands for element activation, while 0 means than an element is inactive.

Firstly, from figure (3.8) it can be noticed that once an element has been activated, it remains active. Also, it can be deduced that element 10008 belongs in the first layer, as it is activated shortly after the start of the analysis. As for element 10023, it belongs to the second layer since it was activated after 100sec, which is equal to the idle time.

From the graphs of figure (3.7) the two heating phases for the deposition of the two layers can be clearly seen at all nodes. It has to be noted that Node 17 has the same coordinates with node 51 from the previous analysis, 1425 with 8939, 10009 with 100026, 10025 with 100536 and 10041 with node 101046. Node 17 has a similar maximum temperature to node 51 from Model-1, while it appears to cool down during the longer idle phases. The same can be observed for the rest of the nodes and there also appears to be comparable accumulation of heat despite the longer cooling times. During the heating of node 10041 the effects of latent heat can be seen as the temperature of the node remains almost constant.

Figure (3.9) depicts the wall part of the model at three different time stamps. One is during the printing of the first layer, b) is during the first idle phase and c) is during the printing of the second layer. From these images it can be observed how focused the heat source is, since the high temperature contours are contained within the elements that are directly under the laser spot. Another thing that can be noted is the rapid diffusion of heat towards the substrate. Image b) is taken just 1.01 seconds after the laser paused and already the whole newly printed layer is below 100°C. This is as expected since the substrate is a major heat sink in this analysis.

Lastly, on the left side the alignment of active nodes and the heat source can be seen. At a) the first six elements of the first layer are active. The first two have already cooled significantly, while the next two are at their peak temperature. So, as expected the laser, whose radius is 0.4mm (the length of two elements), is at that

moment heating the fifth and sixth element.

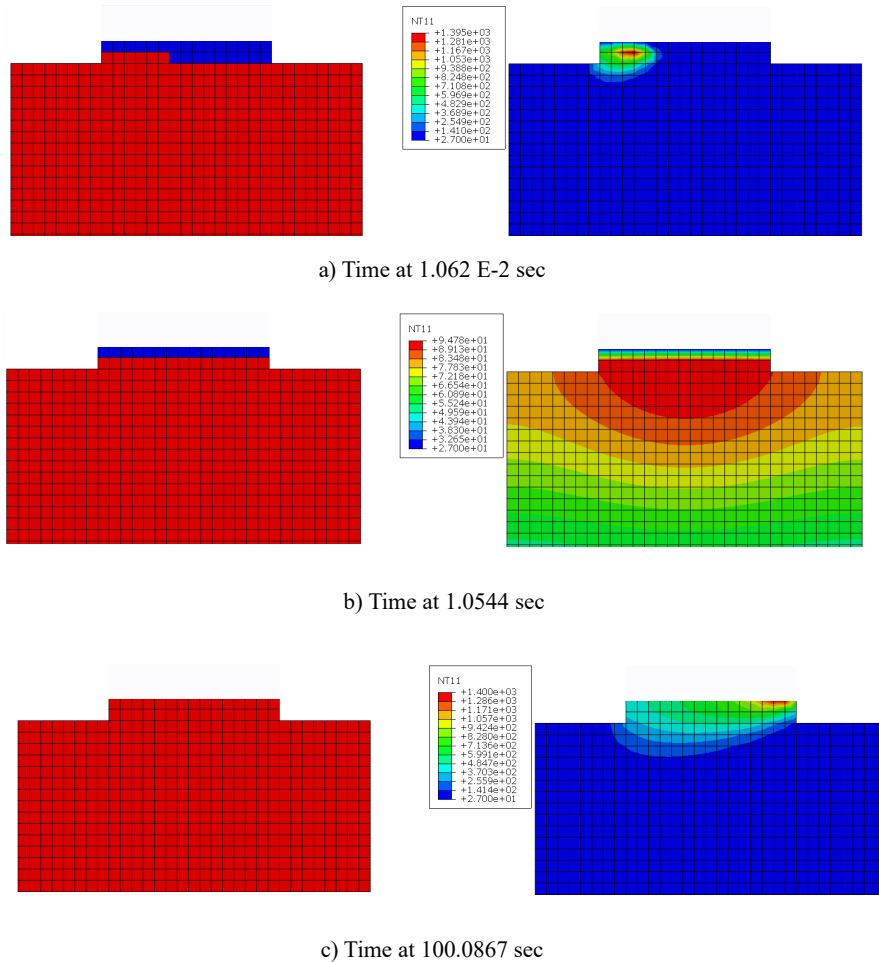


Figure 3.9: Left: Element activation status, where red means active and blue inactive. Right: temperature contours at the same time as the images on the left.

3.5 Complete 2-D Wall: Model-3

3.5.1 Overview

This model has the exact geometry that was discussed at Bertsch, as is displayed in figure (3.10). Relative to the other two models, the substrate has been expanded but the ratio of substrate to printed area is smaller. The energy density, as well as the energy intake per scanning phase are the same as the previous models. A single layer was 0.2mm thick so it accounted for 10 actual layers. A total of 2590 elements were used, 900 of which were assigned to the wall section in order to simulate the creation of 65 layers.

The following parameters are specific to this analysis:

- Laser speed: $v_s=67.5$ mm/sec
- Idle time of the laser: $DTIDLE=100$ sec
- Laser starting location: $(x_0, y_0)=(1,15)$
- Substrate element dimensions: $DX=0.5$ mm and $DY=0.5$ mm
- Wall element dimensions: $DX=0.5$ mm and $DY=0.2$ mm
- Ellipsoid parameters: $a=0.4$ mm, $b=0.2$ mm and $c=1$

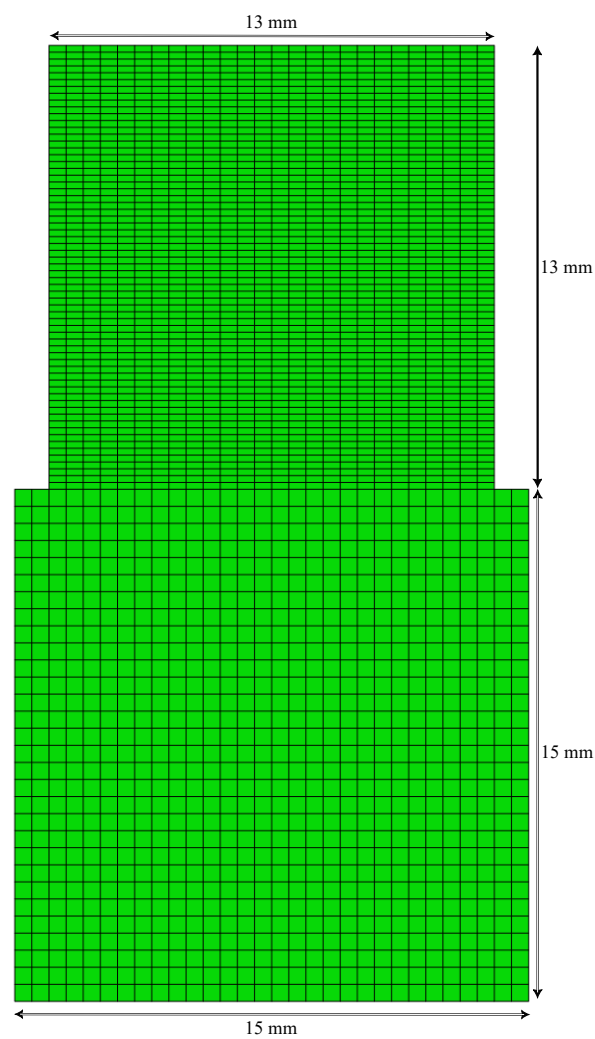


Figure 3.10: Model-3 Geometry

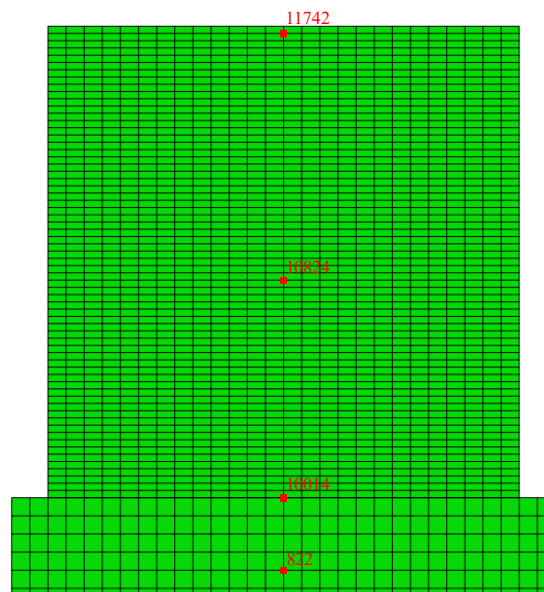


Figure 3.11: Model 3 Node locations

3.5.2 Results from Model-3

The following results are from the nodes whose locations can be seen at figure (3.11), except for node 16, that is at the base of the substrate. All these nodes have the same x-coordinate of $x=7.5\text{mm}$, thus being in the middle of the model.

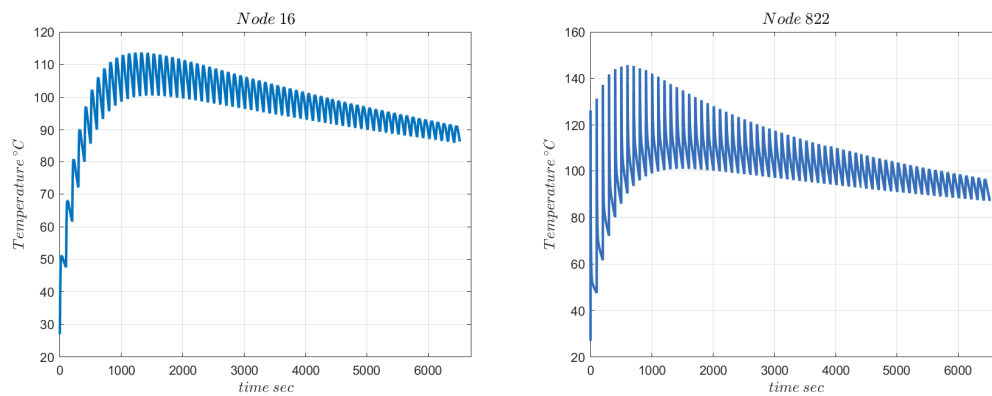


Figure 3.12: Temperature history from model-3 at two nodes of its substrate.

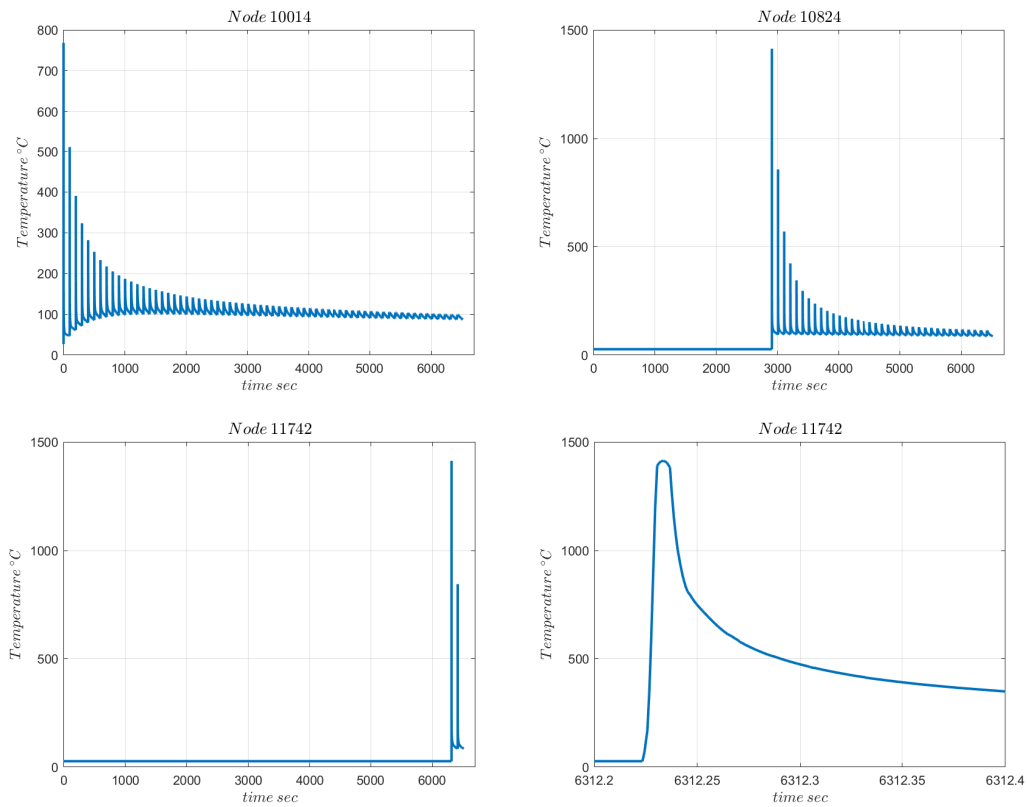


Figure 3.13: Temperature histories at three nodes of the wall section from model-3. The right bottom image is a zoom-in for the first heating phase of node 11742.

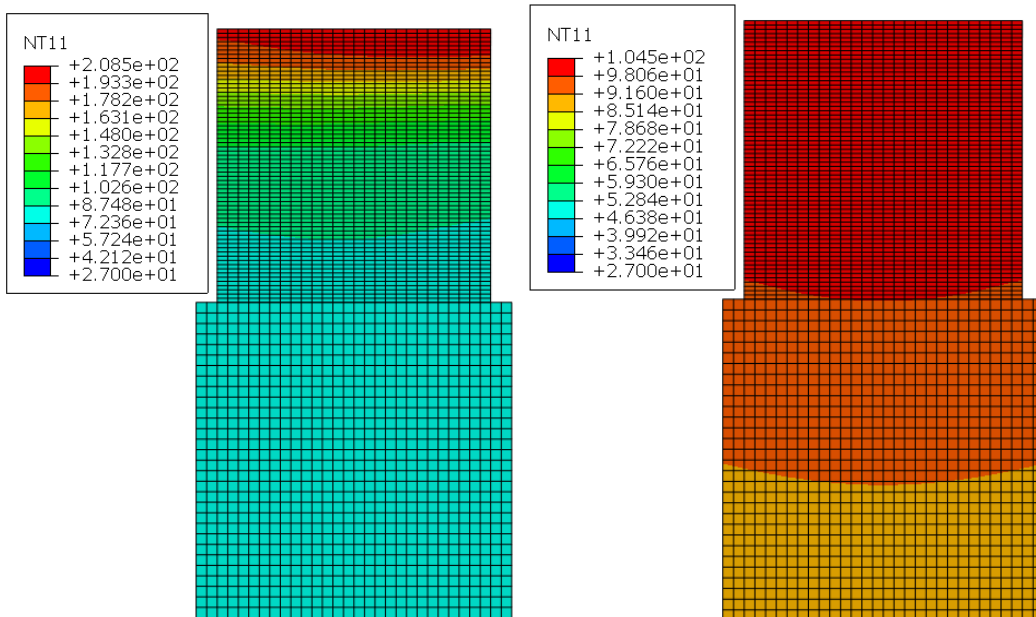


Figure 3.14: Temperature contour plots from Model-3 at different times during the same idle phase.

Based on Figure (3.12) it can be seen that the maximum temperature of the substrate has been increased relative to Model-2. The cause of this is the relatively smaller substrate compared to the printed area of Model-3, so relatively less heat can be dissipated through convection in the substrate. Nevertheless, after about ten layers (1000seconds) the maximum temperature peaks and subsequently starts to decrease with each new layer. The higher temperatures (relative to the ambient temperature) and the constantly increasing surface area of the model, lead to higher heat dissipation via its boundary conditions, which are two of the reasons for this decrease.

At the nodes of the wall, it can be observed that the maximum temperatures during each pass of the laser, are approximately the same as in Model-2, since the same parameters apply concerning the heat source (laser speed, ellipsoid parameters and layer thickness). It should also be noted that in the wall area, there is a relatively steady minimum temperature of 100°C.

Figure (3.14) on the left, shows how fast the temperature has dropped at the newly printed layer. This cooling phase began 0,865 seconds before this contour plot and the temperatures there are at 200°C. The right image of Figure (3.14) is 23 seconds later than the left one and the effects of the saturated heat sink can be seen there, since the temperature on the wall has decreased only by 100°C from what was observed on the left figure. This can also be displayed on the fourth image of figure (3.13), after the heating phase, there is initially a sharp decrease of the temperature, followed by constantly decreasing cooling rates.

3.6 Simulating the Effect of Metal Powder: Model-4

3.6.1 Overview

The previous three models had a common re-occurrence concerning the maximum temperature at each new layer and that was that they narrowly reached the $T_{Liquidus}$ of steel 316L. With this in mind a fourth model was created.

The main modification of this model is that it takes into account the metal powder. When the heat source first engages with an element, its properties are now swapped for those of metal powder as this was explained in Chapter 2. The boundary conditions have also been changed for this model, the convective and radiation losses are only considered at the top surface, while at every other boundary, a conductive heat loss through a semi-infinite metal powder medium was assigned, as explained in subsection (2.3.5). No substrate was considered and all 1000 elements were assigned to the wall area, in order to simulate the printing process using the physical values for the layer

thickness.

The following are parameters specific to this analysis:

- Laser speed: $v_s=675$ mm/sec
- Idle time of the laser: DTIDLE=10 sec
- Laser starting location: $(x_0, y_0)=(0,0)$
- Element dimensions: DX=0.02mm and DY=0.02mm
- Ellipsoid parameters: a=0.04mm, b=0.02mm and c=1

3.6.2 Results from Model-4

These results have been taken from nodes whose location can be viewed at figure (3.13) and their coordinates are Node 26 (0.5,0), Node 77 (0.5,0.02), Node 485 (0.5,0.2) and Node 944 (0.5, 0.38).

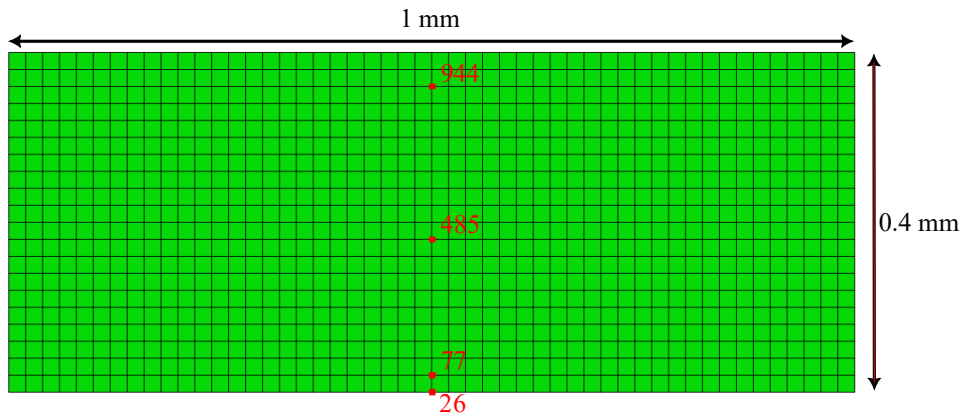


Figure 3.15: 13 Model-4 geometry and node locations

From figure (3.16) it can be seen how elements are activated based on their relative location to the heat source, firstly as powder elements and then as proper metal elements. Figure (3.17) shows this alternation more accurately. The two top images of that figure are from an element belonging to the first layer. It is initially activated from the beginning, as an element with powder properties and once the heat source has moved past it and it begins to cool down, it immediately alters its active state to that of an element with proper steel 316L properties. The bottom two images show an element at the ninth layer, which was initially inactive, then briefly it was activated with powder properties for part of the scan duration, until its active state was altered with proper metal properties and remained unchanged throughout the rest of the analysis.

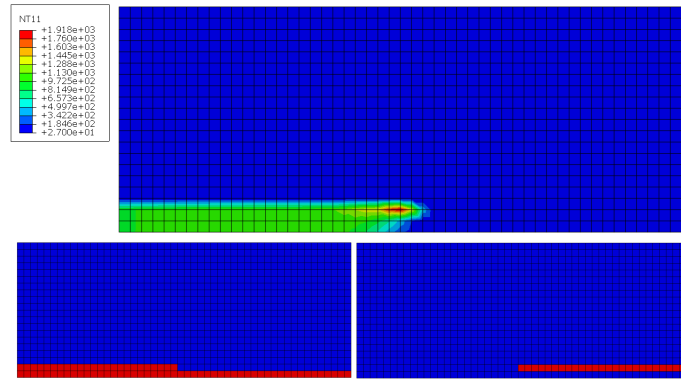


Figure 3.16: Model-4 at time = 10.0022 seconds. Top: temperature contours. Bottom left: elements with red are active with solid properties. Right: elements with red are active with powder properties.

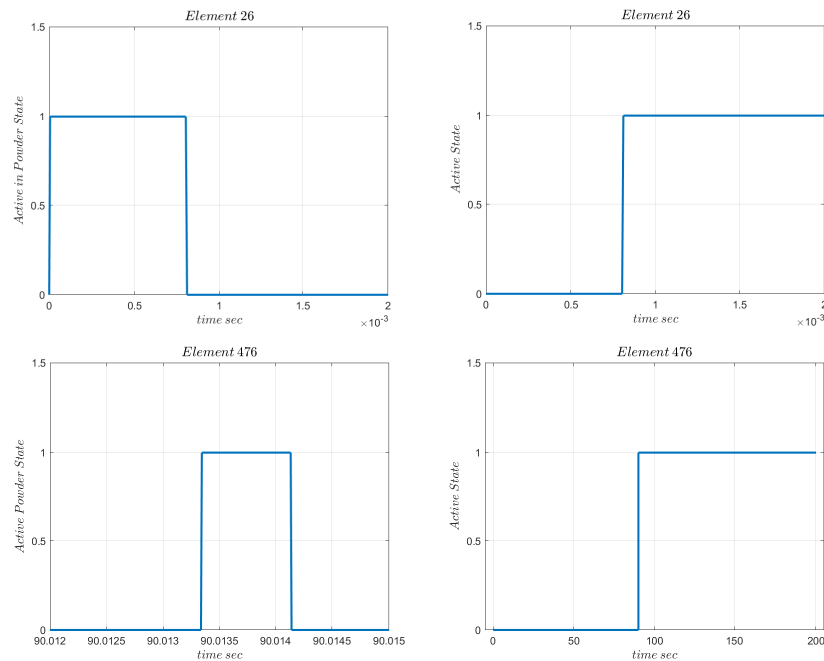


Figure 3.17: Time graphs showing the state of two elements, element 26 at the top and element 476 at the bottom. On the left is their status as active elements with powder properties, while on the right is their status as active elements with proper metal properties.

The temperature contours from figure (3.18) show that the heat source retains its focused nature and also that diffusion through conduction still has an important role for the rapid cooling of the built specimen during the idle phase. Also, the temperature-time plots of figure (3.20) show a significant rise of the maximum temperature a node experienced during the heating phase. Now, the nodes temperature rises up to 2000°C, well over the liquidus temperature of 1430°C. Similar to the previous models this heating is followed by a brief period of rapid cooling. This time however, the minimum temperature is around 200°C, which can be explained by the lack of a substrate, that

acts as a major heat sink for the printed wall.

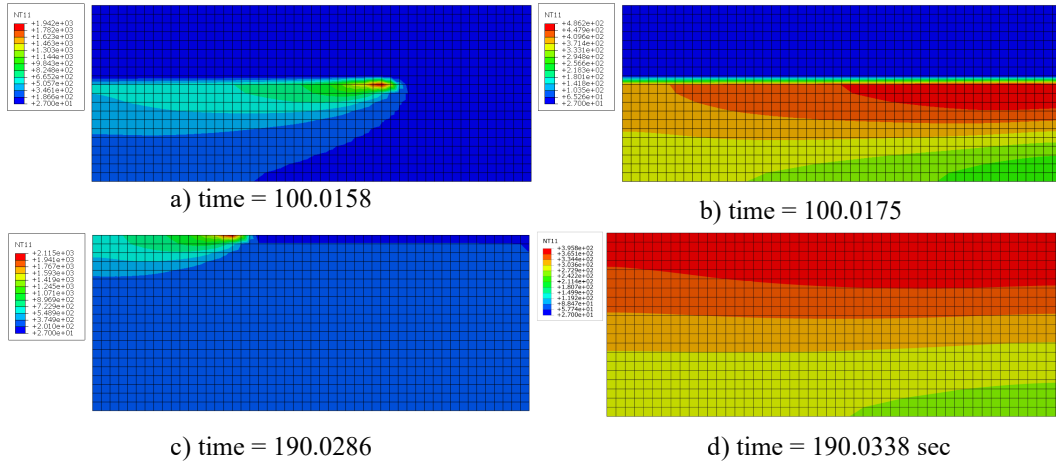


Figure 3.18: Contour Plots of model-4 at different times

Another useful piece of information can be obtained from figure (3.21), which shows the first heating of Node 485. The element this node belongs to was active (with powder properties) from the start of the heating phase of the ninth layer and is located in the middle of it. The heating of that layer began at $t = 80.01185$ sec and in the graph a slight heating of that node can be seen until 80.0125, when the heat source is directly above it and it begins its proper heating. This very slight initial temperature rise shows that while the heat source is active and moving it is the main influence on the thermal field's distribution on the x-axis, while heat conduction has a negligible effect on the x-direction during that time. The reason for this is the significant travel speed of the heat source.

Lastly, an interesting phenomenon can be observed at Figure (3.21) and that is the phase change of the material. Once, the heating of the nodes starts, it occurs at a rapid pace, yet once the temperature reaches the value of $T_{solidus}$ and a liquid phase begins to form, this rate is hampered. This is due to the absorption of energy by the material in the form of latent heat, as described during section 2.3.2. Once the temperature has surpassed $T_{liquidus}$, rapid heating resumes, with the difference that this time the material inside the element is in a liquid state. This occurs in the opposite fashion during the cooling phase, where the phase change process delays the major cooling rates.

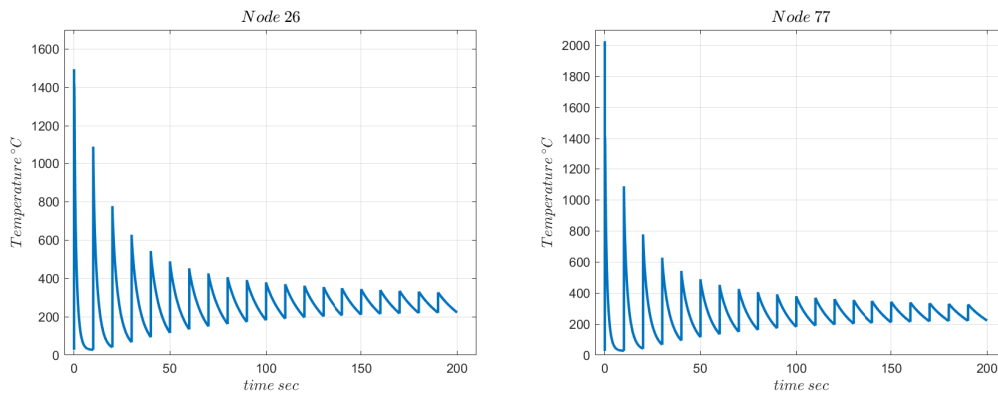


Figure 3.19: Temperature history of nodes 26 and 77.

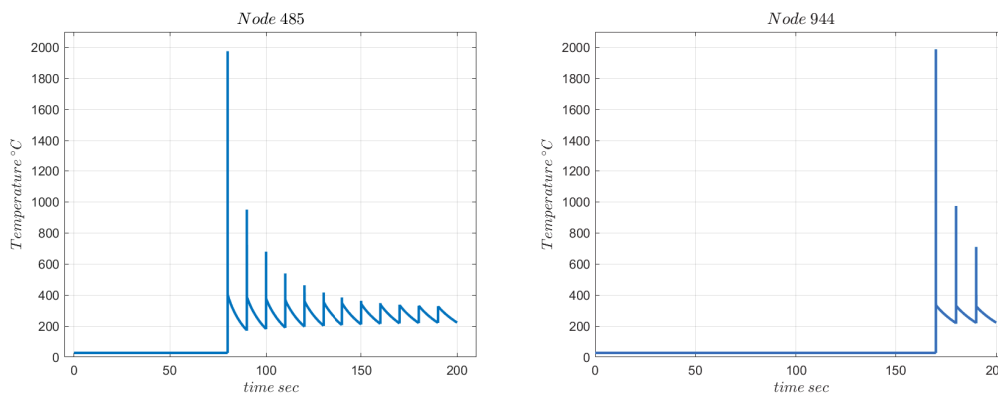


Figure 3.20: Temperature history of nodes 485 and 994.

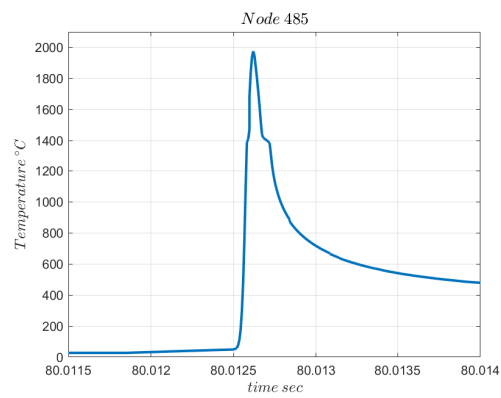


Figure 3.21: First heating at the node 485.

Discussion and Conclusions

Throughout this thesis, a finite element model was employed in order to simulate the evolution of the temperature field, which is produced as a two-dimensional wall is constructed out of stainless steel 316L, through the SLM method of additive manufacturing. Four different versions of that model were produced, in order to observe how certain modelling parameters, effect the accuracy of the results. Some of these results have already been discussed for each model in the relevant subsections regarding each model, yet the following may be considered as the main conclusions:

- The modified quiet element method yields accurate results and this is derived from the behavior of the very first heating cycle that a node experiences. As soon it is activated, it rapidly heats due to the presence of the heat source and subsequently cools down once the laser moves away from its region. This is further reinforced by the results of Model-4, where the elements of the printed layer are preemptively activated with the properties of powder and only obtain proper metal properties after the laser has moved on from the area of the element. Their temperature history during the first heating had a similar behavior to that of the previous models, regarding the beginning of the heating, which occurs when an element enters the area of the volumetric heat source.
- Despite the limited heat sink in the form of the substrate for models 1,2 and 3, or the lack thereof for model 4, there seems to be limited heat accumulation in the printed part. For all models it was observed that temperatures after some initial heating cycles reach a steady minimum temperature around, 100°C or 200°C in Model-4. As for model 3, where 65 layers were printed (three times more than the other models), it was observed that as the area of the printed part increases, its minimum temperature begins to decrease. These observations emphasize the significance of the convection and radiation boundary conditions, as they introduce significant heat losses to the analysis. The conductive boundary condition with the powder bed, of model 4, displayed similar results and effectively dissipated heat from the wall to the powder bed.

- More specifically, for model 4, adding the powder state to the elements yielded significant results, regarding the temperatures which develop during the material deposition phase (first heating of an element). The metal powder proved easier to heat and thus reached higher temperatures.
- The modeling of latent heat was also working as intended and had visible effects on the heating and cooling rates during the temperature range of $T_{solidus}$, $T_{liquidus}$, making its consideration a vital part of the model.

Regarding Models 1 and 2, the following can be reported:

- Both of these models displayed very similar maximum and minimum temperatures at the nodes of the wall. This may be attributed to the fact that they were designed using the same energy density and total energy input. So, in this regard the change in laser travel speed and layer thickness produced comparable results.
- However, these different settings (speed and layer thickness), lead to dissimilar heating and cooling rates. Model-1 had higher rates both for cooling and heating, compared to Model-2. This is expected to cause distinct thermal stresses to develop for each model and also have different metal phase distributions once they cool down.

Despite this, Model-3 showed that simulating more layers provides valuable information about the thermal cycling patterns that may develop. An example of this being the aforementioned decrease in the minimum temperature at each cycle. Simulating this number of layers was mainly feasible, due to the computational simplification that comes with accounting for multiple layers at once.

Model-4 showed a lot of promise with its novel boundary conditions. Should they prove to accurately account for the presence of a heat-sink, then the computational model shall be significantly unburdened as there will be limited need for the inclusion of a substrate.

All these models however, had an important shortcoming when it came to modelling the layer remelting, which is crucial for producing high density parts through the SLM method of additive manufacturing, as noted by Ahmed. It is expected that the melt pool will extend to the previous layer as well, in order to produce a more homogeneous and finer micro-structure and prevent the formation of pores. As can be seen at the temperature history graphs for all models, the second pass of the laser above a node, only heats it to around 1000°C.

- The use of the simple ellipsoidal heat source has been reported to lead to an underestimation of melt pool's depth, as was recorded by [12] and [13]. So, it would be of great interest to use the same models, but with a different volumetric heat source and measure the differences in the size of the melt pool which forms.

- The density of the material was assumed to remain steady, despite the significant changes in temperature. Its change is especially important inside the melt pool, since a major drop in density occurs during the phase change. So, accounting for the change of material density could also prove an addition with similar results to that of the powder state.
- The Marangoni effect was also not taken into account inside the melt pool. Its inclusion to the model would likely affect the dimensions of the melt pool. On a basic level, its effects were proposed to be modeled by [14] and [12], as an increase to the conductivity of the metal inside the weld pool. This can be expected to lead to greater propagation of heat inside and around the melt pool.

Bibliography

- [1] Yunus A. Cengel, Heat and Mass Transfer, McGraw-Hill (5th edition), (2015)
- [2] Theodore L. Bergman, Adrienne S. Lavine, 'Fundamentals of Heat and Mass Transfer', John Wiley Sons (8th edition), (2017)
- [3] ABAQUS, Analysis User's Manual, Version 6.14, © Dassault Systèmes, 2014
- [4] Spyrou L.A., Aravas N., 'Thermomechanical Modeling of Laser Spot Welded Solar Absorbers', Journal of Manufacturing Science and Engineering, (2015), 137,1–16
- [5] Goldak J., Chakravarti A., Bibby M., 'A new finite element model for welding heat sources', Metallurgical Transactions, (1984),15,299-305
- [6] Gouge M., Heigel J., Michaleris P., 'Modeling forced convection in the thermal simulation of laser cladding processes', International Journal of Advanced Manufacturing Technology, (2015),79,1-4
- [7] Sih S., Barlow J., 'The prediction of the emissivity and thermal conductivity of powder beds', Particulate Science and Technology (2004),22,4
- [8] Bertsch K., MERIC G., Kuehl B., 'Origin of dislocation structures in an additively manufactured austenitic stainless steel 316L',Acta Materialia, (2020), 199
- [9] Sotiriou M., Aristeidakis J., Tzini M., Papadioti I., Haidemenopoulos G., Aravas N., 'Microstructural and Thermomechanical Simulation of the Additive Manufacturing Process in 316L Austenitic Stainless Steel', (2021)
- [10] Kim C.S., 'Thermophysical Properties of Stainless Steels', Argonne, IL, USA, (1975)
- [11] Ahmed N., Barsoum I., Haidemenopoulos G., Al-Rub R., 'Process parameter selection and optimization of laser powder bed fusion for 316L stainless steel: A review', Journal of Manufacturing Processes, (2022),75
- [12] Hocine S., Van Swygenhoven H., Van Petegem S., 'Verification of selective laser melting heat source models with operando X-ray diffraction data', Additive Manufacturing, (2021),37
- [13] Unni A., Vasudevan M., 'Determination of heat source model for simulating full penetration laser welding of 316 LN stainless steel by computational fluid dynamics', Materials Today: Proceedings,(2021)

- [14] Ali H., Ghadbeigi H., Mumtaz K., 'Residual stress development in selective laser-melted Ti6Al4V: a parametric thermal modelling approach', *International Journal of Advanced Manufacturing Technology*, (2018), 97(5-8)